Chapter 15
Characterization Techniques for Nanotechnology Assisted Edible Food Packaging

Deepshikha Das, Tabli Ghosh, and Vimal Katiyar

15.1 Introduction

The nanotechnology is a branch of science which deals with the nanoscale (range 1–100 nm) materials and is used in enhancing the attributes of microscopic and macroscopic materials. It is a booming area of technological advancement, where novel techniques and methods are used to fabricate nanodevices and nanobiomaterials [1]. These kind of nano-based materials are initially applied for developing microscopic devices in the electronic industries. Additionally, the nanostructure materials providing several noteworthy properties such as high surface-area, high strength, better diffusivity and catalytic properties, etc. are targeted for various multifaceted advanced application. In this regards, the development in the area of nanocrystalline materials are also being explored for edible food packaging application in relation to mechanical properties such as ductility and high strength, physicochemical, biological properties (biocompatibility and biodegradability) and microbiological properties. The different grain sizes of nanomaterials have been used by the physicists and chemists to produce novel materials [2]. The property of nanomaterials which are useful in food packaging industry depends on various factors such as particle-size, surface properties, improved bioavailability, dispersibility, water permeability, thermal stability and its antimicrobial property [3]. These properties determine the effect of nanomaterials upon human health and therefore it is utmost essential for proper characterization of the nanomaterials to understand the interaction of these with the environment and ensure their safety usage in the field of edible food systems [4]. The field of nanoscience aims to

D. Das · T. Ghosh · V. Katiyar (✉)
Department of Chemical Engineering, Indian Institute of Technology Guwahati, North Guwahati 781039, Assam, India
e-mail: vkatiyar@iitg.ac.in

T. Ghosh
e-mail: tabli@iitg.ac.in

V. Katiyar and T. Ghosh, *Nanotechnology in Edible Food Packaging*,
Materials Horizons: From Nature to Nanomaterials,
https://doi.org/10.1007/978-981-33-6169-0_15

develop novel nanostructures in different forms such as nanocomposites, nanoemulsions, nanocapsules, nanospheres, and nanofibers in order to enhance the flavour, texture, shelf-life, and the colour of the food [5]. Recent reports and researches reveal that the use of nanomaterials will lead to a newer and smarter form of packaging system ensuring the safety aspect of the food materials [5].The various techniques involve for the characterisation of the nanomaterials are scanning electron microscopy (SEM), transmission electron microscopy (TEM), high resolution transmission electron microscopy (HRTEM), atomic force microscopy (AFM), scanning tunnelling microscopy (STM) that provide the size and shape of the nanomaterials. The interaction of these materials with the electromagnetic radiation helps to know about the concentration, size, crystal structure, and morphological behaviour of the nanomaterial as a function of its wavelength. This can be achieved by Raman spectroscopy, ultraviolet visible (UV-Vis) spectroscopy, attenuated total reflectance Fourier transform infrared spectroscopy (ATR-FTIR), dynamic light scattering spectroscopy (DLS), Zeta-potential spectroscopy, and X-ray photoelectron spectroscopy (XPS). There are several other techniques used for the analysis of specific materials (magnetic nanomaterial and nanogels) are Vibrating sample magnetometry (VSM), X-ray magnetic circular dichroism, etc. These are related to both physical and structural characterization [6].

15.2 Characterization of Nanostructured Materials

The characterization of nanostructure materials mainly depends on the size and shape, surface chemistry, aspect ratio, hydrophobicity, and other factors. The properties of the nanomaterials vary according to the changes in the sizes of the matter. These are basically layered films and possess different physical and chemical properties as compared to the macrostructured materials with similar chemical fabric. These kind of materials possess vivid potential to create novel inventions with well-designed shapes, structures and crystalline phases leading to the advancement in many areas of sustainable technologies. The different characterization techniques described for the analysis of nanomaterials are quite challenging being interdisciplinary in nature [6].

15.2.1 X-Ray Diffraction

It is a non-destructive technique used for determining the atomic and molecular design of any material. It is the most popular and widely utilized technique for the characterization of the NPs. It gives us a better understanding about the crystalline property of any material. It helps to gain information on the crystalline grain size, nature of the crystalline phase, unit cell parameters, and crystalline grain size. In this technique, the specimen is generally vacuum dried before it is subjected to

analysis. The peak position and intensity of the particles can be determined by comparing with the standard patterns mentioned by the Joint Committee on Powder Diffraction Standards (JCPDS) database [6]. The shape and size variations of any particle is effective in determining the peak intensities of a crystalline material. Upadhyay et al. in the year 2016 reported the structural and magnetic properties of chemically synthesized magnetite NPs (ferric oxide Fe_3O_4) [7], where the X-ray line broadening results showed that the average crystallite size of the magnetic nanoparticles (NPs) are in the range of 9-53 nm and average crystallite size affects the magnetic parameter of the samples. The magnetic parameters of the analysed sample show greater dependence upon the average crystalline size of the material. Besides, Yan and group reported that AuNPs showed higher intensity corresponding to (111) plane than the (220) plane [8]. Additionally, Li et al. prepared CuTe nanostructures with different shapes, where, the relative XRD intensities varied depending upon the shapes of the nanomaterial [9]. In this way, XRD analysis is used to evaluate the chemical composition, and phase identification of crystalline nanomaterials and their modified/functionalized forms via identifying characteristics diffraction patterns.

15.2.2 X-Ray Absorption Spectroscopy

This is a widely used technique for determining the absorption co-efficient of a material which is a function of energy. Here, element transitions of direct energy levels occur from ground-state to the excited-state due to absorption of energy. Each element corresponds to the binding energy of its electrons making itself more selective in nature. In X-ray Absorption Spectroscopy(XAS), generally synchrotrons are used for acquiring the spectral absorption. There are other two methods of absorption that predicts the structural information of the elements. The extended x-ray absorption fine structure (EXAFS) is the most sensitive technique that studies the structural absorption, where the energies are considered greater than the intensity level required for electron release. It also tells about the information regarding the chemical nature of the element by reporting numbers, ligands and nearby atoms from the absorbing element. The x-ray absorption near edge structure (XANES) reports the density of partially filled electronic states of the metal site considering the excitation energy of an inner shell permitted by dipole interaction rules [10]. Many researchers reported XAS to investigate interactions within metals in order to examine several structural changes. Heinz and group (2016) used the HRTEM, XRD, EXAFS, and optical absorption spectra to find out the correlations between the structural and plasmonic properties of silver (Ag) atoms and their NPs aggregates [11]. The EXAFS of Ag K-edge spectra study indicated the atomic structure of Ag-Ag and Ag-O bonds, averaged over neutral and ionic states of Ag [11]. Pugsley et al. (2011) reported the formation of nano-Ge (nano germanium) particles by reaction between dissolved $GeCl_4$ (Ge^{4+}) and suspended Mg_2Ge (Ge^{4-}) in a diglyme solvent. Here *in situ* XAS have been used to study the kinetics

mechanism of the reaction. The EXAFS and TEM analysis can provide the information on the formation of nano-GeO_2 particles. The EXAFS can also reveal the Ge-Ge distance (obtained value: 2.45 Å) by comparing it with the XRD analysis [12]. Chen and his group synthesized the cubic germanium oxide (GeO_2) decorated with sodium bis(2-ethylhexyl) sulfosuccinate (AOT) using the reverse micelle technique. *In situ* EXAFS have been used to examine the structural behaviour around germanium and its atoms in GeO_2NPs. Interestingly, they also observed that at higher temperature, the complete formation of GeS_2 took place due to the presence of sulphur content [13]. Ramallo-Lopez and his co-workers (2007) prepared palladium (Pd) NPs capped with *n*-alkyl thiol molecules and studied the structural and electronic behaviour of alkyl thiol-capped Pd NPs due to the sulphur-Pd interactions. The analysis with the help of XANES and EXAFS revealed the sulfidation of clusters of Pd that is caused by capping thiols, which occur both on the surface and in the bulk [14]. Pizarro et al. (2004) investigated metallo-protein with the help of XAS to evaluate the effect of the coordination charge on the absorption edge energy. The understanding of EXAFS in case of metal systems for unknown structures also provides a criterion for studying well-characterized model systems [15]. The theory of XAS also has been developed in such a manner to help us build understanding of the complicated molecules of known structures as shown by Rehr and Albers [16]. The importance of XAS over the X-ray crystallography provide information related to element structures for both powders and solution based samples. Also, these techniques are most easily applicable for ordered samples such as single crystals. These are specially used for determining structural information from multi-nuclear metal clusters which are linked with water oxidation in the photosynthetic oxygen evolving complex (OEC), such as Mn_4Ca clusters [17]. Cinco et al. (2002) developed another method where EXAFS measurements are used to gather information on both manganese (Mn) and calcium K-edges (Ca K-edges) for the OEC cluster [18]. Sharma et al. (2015) synthesized copper-oxide (CuO) NPs and Cu_2O/CuO and CuO/TiO_2 by a modified co-precipitation method. The combination of these two techniques of XANES and EXAFS evidenced the different oxide phase probing of the local electronic and atomic structure of these samples. Further, XANES provides information on oxidation and local structure of iron atoms. Small angle x-ray scattering (SAXS) technique reveals the information on the size of the particles. The combination of SAXS and XANES studies also helpful to understand the formation of maghemite NPs in water both structurally and chemically [19].

15.2.3 Small Angle X-Ray Scattering

It is an analytical technique used for the measurement of intensities of x-rays at smaller scattering angles (0.1–5°). SAXS is generally used for the determination of particle size distribution and shape. The schematic presentation of in situ setup employed for real time SAXS/Wide Angle X-Ray Scattering(WAXS)/UV-Vis

measurements during the formation of Au nanoparticles (NPs) has been represented in Fig. 15.1. The SAXS analyses for size are statistically quite average than the TEM analysis for size. It is a low resolution based technique because of which in certain investigations, XRD or any other electron diffraction techniques becomes necessary for NPs characterizations. Wang et al. (2008) prepared platinum (Pt) NPs coated with poly(vinylpyrrolidone) (PVP), where they found size of the NPs obtained by SAXS are bigger in size as compared to the images obtained by TEM analysis. This is due to the presence of PVP coating that showed different scattering intensity. SAXS is quite sensitive to the fluctuation of size due to electron density around any particle whereas, XRD is sensitive towards the wider size region. SAXS technique provides the actual particle size while the crystallite size is yielded by XRD. It is important to note that the different size values of SAXS and XRD is basically due to different growth rate of NPs during thermal treatment [20]. Singh et al. (2011) studied the localized surface plasmon resonance (LSPR) behaviour in case of aqueous sols of polyvinyl alcohol (PVA) stabilized AgNPs. SAXS study enabled more quantifiable learning between the LSPR behaviour and the aggregation phenomenon of the correlations. The structure and property relationship is also much feasible since both applies scattering phenomena. Moreover, the size range of these NPs as shown by LSPR is quite similar when compared to SAXS analysis [21]. Bulavin and co-workers (2016) demonstrated a combined approach using SAXS, UV-Vis spectroscopy and QELS (quasi elastic light scattering) to characterize Ag sols in polymer matrices. The SAXS analysis exhibited monomodal scattering size distribution along with QELS and UV-Vis, which showed multimodal particle-size distribution. This is because SAXS uses small x-ray intensities ranging (1–5°), whereas the QELS and UV-Vis employs higher intensity angles with large particles ranging within 30-60 nm. There are some particles that couldn't be analysed as the properties are beyond the detection limits of SAXS. However, all the aforementioned methods were in good concord for analysis of the particle size and polydispersity index (PDI) in the case of relatively smaller size particles [22]. Generally, SAXS helps us to gather information regarding the concentration and size of NPs simultaneously with respect to time function. Liang et al. (2012) studied the process of formation of mesostructured (platinum-ruthenium) Pt-Ru NPs which was electrochemically reduced from their metallic salts and implanted in a microemulsion type of lyotropic liquid crystalline template (MLLC) [23]. A process of comprehensive evolution from metallic precursors to subsequent atom reduction, mesostructure formation and NPs aggregates formation have been studied by using *in situ* XRD, SAXS and XANES technique. Chen et al. developed a process in order to study the nucleation and growth kinetics of AuNPs as a function of concentration, temperature, ligand ratio and solvent type using SAXS, WAXS and UV–Vis spectra techniques [24]. A schematic representation of this has been shown in the Fig. 15.1.

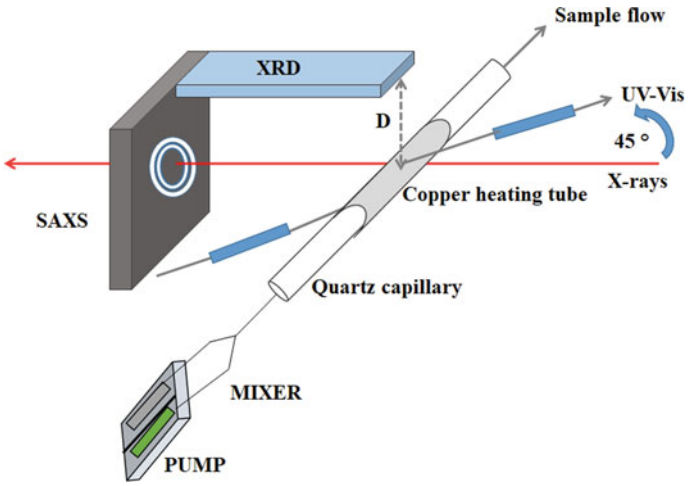

Fig. 15.1 Schematic presentation of SAXS/WAXS/UV–vis measurements during the formation of AuNPs

15.2.4 X-Ray Photoelectron Spectroscopy

It is a surface-spectroscopy analytical technique used for the measurement of elemental composition of the materials. This technique is used for the analysis of nanomaterials and provides information on the nanoscale surfaces. It works under the principle of photoelectric effect [6]. Here, the bombardment of electrons on the metal targets such as aluminium (Al) and magnesium (Mg) targets takes place in order to generate x-rays [25]. It is a technique that is used to explain the chemical analysis of any element, its elemental composition, electronic structure, oxidation states, ligand exchange interaction and surface functionalization of nanomaterials. The x-rays are entirely incident and absorbed by an atom of the material. The electrons that are ejected from the sample depend upon the binding energy of the core electrons of the atoms. If the photon energy is more than the binding energy, the electrons emit from the surface of the elemental surface. The kinetic energies of the ejected electrons can identify the elemental structure of the materials. The XPS technique is quite sensitive to the chemical framework of the atoms as it detects the chemical nature of the elements [5]. In a study related to core-shell NPs, Shard demonstrated direct and empirical method to interpret the shell thickness of spherical core-shell NPs with the help of XPS data [26]. Similarly, Sarma et al. (2013) reviewed the benefit of using XPS in order to study about the internal structure of NPs. While comparing it with TEM and TEM/Electron Energy Loss Spectroscopy (EELS) that uses lateral spatial for characterizing elements which acts perpendicularly to the probing electron beam, whereas, XPS probes act along the direction of electron beam [27]. Barros et al. (2015) used XPS technique to study the surface framework of NPs and also the oxidation of copper species in order to

interpret the degradation of the Amaranth food dye as heterogeneous catalyst by electro-Fenton process. The copper spinel oxides reveal that the copper species are excluded to the NPs surfaces [28]. Also, XPS is a powerful technique to study the proteins and peptides. Belsey et al. (2015) used two approaches for the analysis of protein coatings on the surface of gold (Au) NPs. The XPS study helped to understand the adsorption of proteins on the Au surface. The characterization of the molecular interface was done by analysing the thickness of the NPs coatings [29]. The dielectric properties of nanomaterials can also be analysed with the use of XPS technique. In this regard-, Tunc et al. in demonstrated an easy method for controlling the charge that is developed over Au/silica NPs. The XPS analysis of these NPs helped for the facilitated detection, location and identification of the charges in a non-contact manner [30]. In another work, Prieto et al. (2012) studied the Ag, nickel (Ni) and bimettalic Ag-Ni NPs with sizes less than 35 nm acquired by derived seed-mediated growth method on transparent and conductive indium tin oxide (ITO) substrates by XPS, XRD and optical spectroscopy. The XPS analysis provides the oxidation states of Ag and Ni, where the surface of Ag NPs are not oxidized, and the Ni NPs were oxidized to Ni oxide (NiO) and Ni hydroxide ((Ni $(OH)_2$). It highlights the fact that it could also identify the amorphous species, while XRD failed to detect the peaks for NiO and $Ni(OH)_2$ [31].

15.2.5 Dynamic Light Scattering Spectroscopy

It is a technique used for the analysis of the size of NPs in colloidal suspensions or solution with size ranging from nano to submicrometer ranges. In this, a beam of monochromatic light passes through the sample solution as a laser and the fluctuations occur as a function of photon auto-correlation. The experiment requires minimum sample and its non-invasive, which provides information about the complex behaviour of concentrated polymer solutions. The NPs are dispersed in a continuous Brownian motion. The Stokes-Einstein assumptions are utilised to determine the NPs hydrodynamic diameter. The system pre-conditions the samples in which the calorimetry experiment is performed. The instrument is operated under temperature conditions of 4–60 °C [5], as represented in Fig. 15.2. It is finally connected to the software that depicts the information about the size distribution of various components in the sample. In DLS, a low concentration of the sample is required so as to avoid the multiple scattering effects [32]. The DLS technique is quite sensitive as compared to SAXS analysis. Tobler and co-workers tried to highlight the fact that DLS is much more sensitive towards aggregation of NPs in case of silica NPs(SiO_2). Both the analysis method confirmed the ionic strength and silica concentration for the NPs formation [33]. Lim et al. reviewed the characterization of magnetic NPs with the help of DLS technique. Here they discussed how various factors such as particle shape, colloidal stability and concentration affect the size distribution and colloidal stability of magnetic NPs. Also, by comparing with other sizing techniques such as TEM and AFM, they discussed both pros and cons of using DLS. The self-assembly

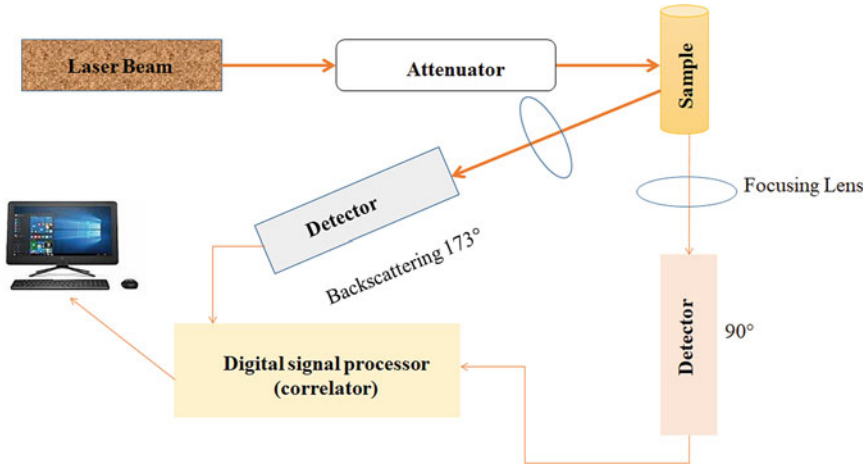

Fig. 15.2 Schematic representation showing the instrumentation of DLS

of the NPs can also be analysed by DLS [34]. The differential calorimetry technique, DLS is well known for its feasible operation for monomodal suspensions. The one limitation for the DLS is its necessity for the samples to undergo Brownian motion. Therefore, in case of polydisperse heterogeneous samples, its resolution is quite low because larger particles scatter more light. Although it measures anisotropic structures that sometimes assume spherical shaped particles, DLS requires transformative assumptions while interpreting data for polydisperse samples [15]. Additionally, the dimensions (average hydrodynamic diameter) of nanoparticles and its aggregates in aqueous suspension can measured using DLS [35]. The nanoparticles having wide size ranges are difficult to analyse by DLS as this technique is less sensitive towards smaller particles. Driskell and co-workers made a novel approach in using one-step screening method for characterizing antibody conjugated AuNPs. The advantage of using DLS as compared to the classic colorimetric technique is to determine the specificity of antibody-antigen aggregates. It also offers an important improvement in comparison to Enzyme-linked immunosorbent assay ELISA (enzyme-linked immunosorbent assay) assays for proteins [36].

Murdock et al. (2007) characterized range of NPs such as metals, metal oxides and carbon-based materials. The cell culture studies along with DLS measurements were used in order to assess the toxicological effects such as agglomeration changes due to the presence or absence of serum in cell culture media. The DLS measurements revealed that the NPs in solution necessarily do not justify their size [37].

15.2.6 Transmission Electron Microscopy

TEM is a high-resolution technique for structural and chemical analysis [36]. Here, an electron beam is transmitted through an ultra thin sized sample and interacts

while passing through it. The TEM facilitates the direct imaging of the structure of the atom of the solid and the surface by collecting information about the size, crystallinity, shape of the particle. It creates a very high-resolution image of approximately0.1 nm. It is also an important tool for chemical analysis as the beam of the electron passes through a very small diameter (>3 nm) of a NPs. When the beam of the electron interacts with the sample, it helps in the determination of some scattered and unscattered electrons [31] which are detected by the detector. The preparation of a sample for TEM analysis is a complex method. The sample must be of very thin in size because the electrons which are directly transmitted through the sample is generally of size less than 150 nm. For a very high resolution, the size must be within 30 nm size range [5]. Dubiel and colleagues reported that EXAFS showed higher accuracy than HRTEM in the determination of lattice parameters in case of Ag NPs embedded in silicate glasses [38].

15.2.7 Raman Spectroscopy

It is a non-destructive chemical analysis technique that is based on the phenomenon of light scattering. In this, the intensity of the scattered light is such that one in a million of the photons will group with the molecular vibrations of the sample and emit diverse wavelengths of light. These low intensity of light when interact with the molecular vibrations results in a shift of the photon energy [39]. The shift energy comes into effect, when the laser beam of light interacts with the electron cloud of molecules [40]. The entire process depends upon the inelastic scattering of the monochromatic light rays which is known as the Raman scattering. The Stokes Raman effect is generated when a molecule gets energized from the ground state level to a virtual energy state level and then relaxes back into the vibrational excited state level [41]. The studies of superparamagnetic $NiFe_2O_4$NPs prepared by sol-gel auto-combustion method is characterized by Mossbauer, Raman and X-ray analysis. The study reports about the single-phase nanosized $NiFe_2O_4$ with average crystallite size of 9 nm showed superparamagnetic properties. The Mossbauer spectra study showed that the NPs consisted of mixed spinel structure and canted spin order at 5 K, whereas the bulk particles depicted collinearity in order with perfect inverse spinel structure. The sizes of the particles were controlled by maintaining the heat treatment temperature. The results based on X-ray diffraction, Raman and Mossbauer analysis concluded that the particles are in a single phase with this process of preparation. The significant broadening and shifting of the Raman bands of the NPs with decreasing of the particle are also observed [42]. The surface enhanced Raman spectroscopy (SERS) technique is quite sensitive analytical method for detecting or quantifying trace amounts of pesticides in raw vegetables and fruits [43].

15.2.8 Fourier Transform Infrared Spectroscopy

It is a method of analysis which is based on the measurement of the absorption of electromagnetic radiation with wavelengths ranging (4000–400 cm^{-1}). In this, the infrared light rays falls into the prism in such a manner that the molecule absorbs the IR radiation and becomes active due to the modification of the dipole moment. The spectrum is then recorded which depicts the position of the bands and specific functional groups; providing information of molecular structures and interactions [15]. This technique is an efficient tool for fingerprinting method. It is also used for analysis of nanomaterials and various other materials [5]. Shukla et al. (2003) reported FTIR analysis of ferrous-platinum (FePt) NPs to examine the surfactant bonding in presence of oleic acid and oleylamine [44]. FTIR spectroscopy is generally used to analyse multifunctional NPs and polymer samples having different groups of stretching peaks that is related to aforementioned molecules. Table 15.1 shows a selected few infrared vibration ranges for some of the most common groups generally found in case of NPs [45]. The attenuated total reflectance (ATR) technique challenges the new aspects of the infrared analysis such as sample preparation and spectral reproducibility. It aims for both solid and liquid sampling by faster sampling, reproducibility and minimising spectral variance. Shankar et al. studied the FTIR analysis for Ag nanocomposite films with polylactic acid and lignin and recorded the spectra for 32 scans per sample at a resolution of 4 cm^{-1} [46] and similarly studied for chitin nanofibril-reinforced carrageenan nanocomposite films using ATR-FTIR technique with frequency range 4000–500 cm^{-1} [47]. A combined approach of thermogravimetric analysis (TGA) technique with FTIR study on the effect of magnetic cellulose nanofibers (mgCNF) on chitosan (CS) based edible nano-coating showed the development of different gaseous components at various IR ranges within 4000–450 cm^{-1}. The appearance

Table 15.1 The infrared vibration ranges and their corresponding functional groups for NPs

Frequency range (cm^{-1})	Functional groups
2970–2950 or 2880–2860	Methyl C–H stretching (asym./sym.)
1680–1620	C=C alkenyl stretching
3130–3070	Aromatic C–H stretching
3400–3380, 3345–3325	N–H aliphatic primary amine, NH stretching
1650–1590	N–H primary amine, NH bending
3570–3200 (broad)	O–H hydroxyl group
1470–1430 or 1380–1370	Methyl C–H bending (asym./sym.)
1050	C–O stretching
1090–1020	C–N, primary amine, CN stretching
1050–990	Aliphatic phosphates (P–O–C stretching)
1365–1340 or 1200–1100	Sulfonates
800–700	Aliphatic chloro compounds, C–Cl stretching

of smaller amount of gaseous products during the analysis of mg-CNFs provided a route for the usage of melt-extrusion technique, blown film technique and injection molding in case of biodegradable films. Here, the iron mound NPs paved a way for developing sustainable materials for food packaging applications which is related to evolution of fewer greenhouse gases [4].

15.2.9 Atomic Force Microscopy

It is a microscopy technique used for creating three dimensional images of NPs surfaces at higher magnification. It was developed by Gerard Binning and Heinrich Rohrer at IBM research laboratory in the year 1986 [48]. It is designed to measure the friction, magnetism, and height of the sample. In this AFM, it is conducted between the probe and the sample as a function of their mutual separation. This method can be used to find the sample's Young's modulus. The probe is like a sharpened tip which is connected towards the end of a cantilever, made of silicon nitride. AFM can scan under different modes between the probe and the sample i.e. contact, non-contact and tapping (intermediate or oscillating mode) method [5]. The tapping mode is most common for characterizing the NPs. Additionally, there are other parameters that influence the final topological values such as tip curvature radius, and surface energy and elasticity of the NPs. A representation of AFM set up has shown in Fig. 15.3. Alternatively, non-contact method is preferred in case of sensitive sampling and can be influenced by tip-sample forces [5]. AFM technique can also be used for measuring other properties such as imaging, mechanical properties such as stiffness, electrical and conductivity properties. This technique has the advantage of not requiring surface modification or coating prior to the analysis of the sample. The topological analysis of ion-doped Y_2O_3NPs (≤ 6 nm) performed by AFM did not require any prior modification before analysis [5].

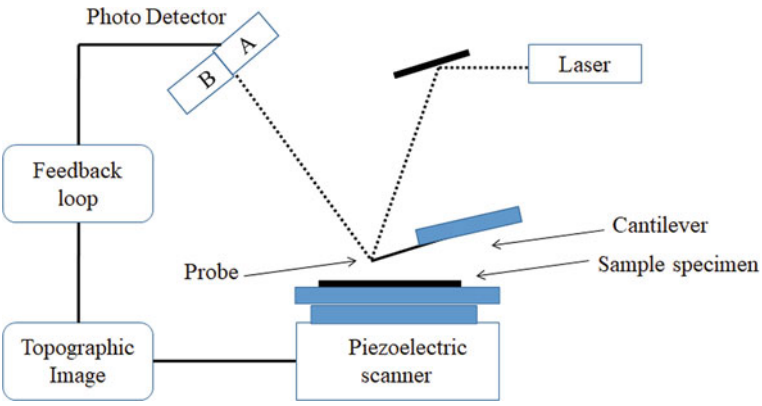

Fig. 15.3 Representation of AFM set-up

Further, AFM has been used to study the formation mechanism of uniformly patchy, hollow and rectangular shaped nanoplatelets made of polymer mixtures [49]. De Moura et al. (2012) reported AFM images of AgNPs for an antimicrobial effect of cellulose-based active food packaging, in a contact mode, by using silicon nitrate tip with a spring constant of 0.06 N/m [50]. Dhar et al. (2016) reported the fabrication of four varieties of cellulose nanocrystals (CNCs) through acid hydrolysis and its effect on the mechanical, thermal and surface properties of polylactic acid bionanocomposite films [51]. The morphological study of the different CNCs in terms of length, diameter and aspect ratio can be evaluated using FESEM and AFM micrographs.

15.2.10 Scanning Electron Microscopy

It is a widely used imaging technique employed for the characterization of nanomaterials. The SEM uses the electrons for imaging the surface of any material instead of light as involved in light microscopy. The image resolution depends on the interaction between the specimen and the electron beam. At times, due to aggregation of particles, the NPs of the sample becomes infeasible to differentiate. When an incident beam of light strikes the sample, the interaction of atoms with its surface leads to the formation of secondary electrons or back-scattered electrons and special X-rays depending upon the surface morphology and chemical framework of the sample. The back-scattered electrons reverted from the sample is responsible for the formation of an image of the sample. The SEM analysis forms a very high resolution image (HRSEM) that can capture size range up to 5 nm. The HRSEM is able to find the nanoscale features of the nanostructured material respective to their properties and application. The SEM is used to analyse the surface morphology of polymer nanocomposites, NPs, nanofibers, and nanocoating. In classical SEM, a beam of monochromatic electrons emitted is generally condensed and accelerated by accelerating anode [5]. Mazzaglia et al. (2009) studied the combined system by using field emission SEM (FESEM) and XPS measurements for AuNPs/amphiphilic cyclodextrin. The morphological information depicted the nature of interaction between (thio hexyl carbon chain) $SC6NH_2$ and (thiohexadecyl carbon chain) $SC16NH_2$ with AuNPs onto the silicon surface [52]. De Britto et al. reported the morphological and particle size study of N,N, N-trimethyl CSNPs as a vitamin carrier system [53]. The NPs are casted on the microscopy slide on top of the specimen stub, which was further Au coated in order to make it conductive and to avoid the disturbance in the sample due to the electron beam. The images revealed smooth and spherical morphology of the NPs. Additionally, Fig. 15.4 depicts the schematic representation of SEM instrument.

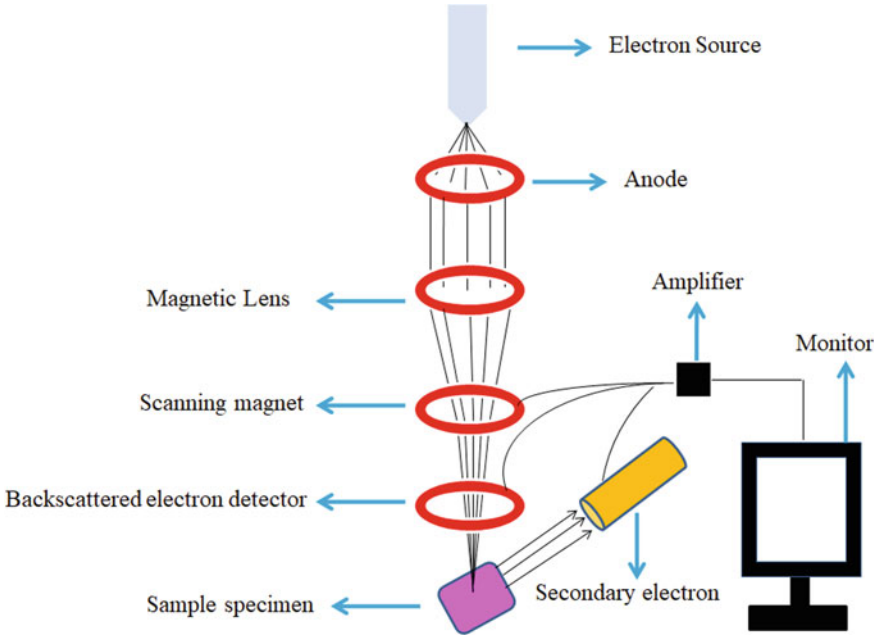

Fig. 15.4 Representation of FESEM set-up

15.2.11 Nuclear Magnetic Resonance

It is one of the techniques used for the quantitative and structural determination of nanomaterials. It is based on the phenomenon that in presence of strong magnetic field, the nuclei possess non-zero spin that causes differences between 'spin up' and 'spin-down' energy states. NMR spectroscopy is generally used to study the interactions of diamagnetic or anti-ferromagnetic NPs. This method does not employ for characterization of ferri- or ferromagnetic materials as wider saturation magnetization causes shift in the signal frequency and relaxation times. As a result of this, a prominent broadening of the signal peaks occurs showing the measurements practically infeasible to be interpreted [15]. A review on NMR techniques for noble metal NPs have been studied by Marbella and Millstone [54]. The report depicted the usage of NMR in various areas and how it will help towards molecular scale investigation of formation of NPs and its morphology in situ. It is particularly useful for analysing both formation and final characteristics of noble metallic NPs. Besides, easing to study the chemical evolution of precursors of ligands, the NMR is also used to investigate the work of capping ligands for particle shape determination [54]. The proton ^{1}H NMR chemical shift is totally sensitive towards the surrounding electronic environment; electronic structures, and bonding environment of the nucleus. This results change in neighbouring spin positions due to the changes in the chemical shift which helps to assess chirality of nanoclusters. NMR

is also favourable for the measurement of hydrodynamic radius of metal NPs in relation to the other available standard techniques such as TEM and DLS. Similar to DLS, NMR spectra are used to determine particle diffusion of NPs. NMR also helps to extract diffusion coefficient of well dispersed species according to Brownian motion and the hydrodynamic size of the particles can be calculated through Stokes-Einstein equation. It is important to note that NMR analysis in case of polymer hybrid particles can only exceed size up to 100 nm and in case of metallic NPs, the dimensions include up to 1–5 nm [55]. Hens and Martins (2013) reviewed a tool for the investigation of surface chemistry of colloidal NPs using proton ^{1}H NMR analysis [56]. A study reported the analysis of AuNPs where ^{2}H NMR was used to characterize the intramolecular ligand dynamics in *d15*-(PPh3)-capped AuNPs. The ^{2}H NMR is known for its simplicity and capacity to differentiate dynamics in both amorphous and crystalline domains in case of organic compounds that are isotropically deuterons [57]. In this regard, Smith et al. used NMR to study the extent of ligand exchange between definite kinds of thiolated molecules on the surface of AuNPs [58].

15.2.12 Vibrating Sample Magnetometer

It is an analytical technique used to determine the magnetic property of materials. It is used to record the magnetization field, magnetic hysteresis loops for magnetic nanomaterials, where different parameters in the form of saturation magnetization (M_S) and the remnant magnetization (M_r) are obtained. The magnetic properties of NPs are studied as a function of its magnetic field, temperature and time. Upadhyay et al. (2016) reported the characterization of synthesized magnetic NPs using XRD, TEM, and VSM analysis. The magnetic parameters showed that the magnetic properties are depended upon the average crystallite size of the material and the ratio of the coercive field at 20 K to 300 K increased sharply with the decrease in crystallite size [7]. Ghosh et al. successfully fabricated mgCNF for edible food packaging through a single-step co-precipitation route, where the iron (Fe) particles are adsorbed onto the surface of CNF. The VSM analysis of the samples revealed that the nano-coated materials depicted magnetic hysteresis, from which it could be inferred that the there is a loss in their superparamagnetic properties and further loading of mgCNF maintained their magnetic properties [4]. Andrade and group prepared size-controlled magnetite NPs using direct reduction-precipitation method in the presence of tetramethyl ammonium hydroxide. The examined samples are found to be superparamagnetic in nature as shown by the zero coercivity and zero remanence on the magnetization loop. The saturation magnetization was found to be a linear function of the size of the NPs [59].

15.3 Characterization of Edible Films and Edible Coatings

An edible film or coating is defined as a thin, continuous layer of edible material developed from edible components on food products. The aim of edible food packaging is to produce natural biopolymer based coated films with specific properties, which may be consumed with the food. The basic function of edible film or coating is to provide a barrier against the transfer of water, gas and lipids; to serve as a carrier of food ingredients and additives (pigments, flavours and so on) and to provide mechanical and thermal stability.

15.3.1 Film Thickness

The film thickness is considered as a crucial parameter for the calculation of mechanical properties and water vapour permeability (WVP). The thickness of films and coatings depends upon the preparation method, sample quantity, and drying conditions. The effectiveness of thickness on edible films property have been reported by many authors. In this regard, the measured thickness of sodium alginate (ALG) and pectin composite based films is used to determine the physical property of the edible films, where, the thickness of the films are measured using electronic gauge with a precision of 1 μm. Simultaneously, five thickness measurements are done at the central and at the four corner of the films, where a mean value was determined and reported [60]. However, the ALG-pectin films thickness changed significantly ($p < 0.001$) from 12.5 to 26.8 μm depending upon the composition of the film-forming mixture. The higher amount of pectin can enhance increased thickness of the composite films. The increased amount of pectin can provide increased thickness of the composite films. Also, da Silva et al. (2009) analysed the amount of glycerol effect on ALG-pectin films having a thickness of 45–70 μm [61]. García et al. measured the film thickness of using SEM analysis, where a correlation was also found between the thickness of the reported chitosan-starch (CS-starch) films, which affected both barrier and the mechanical properties [62]

15.3.2 Barrier Properties

The barrier properties determine the ability of the edible films to improve the shelf life property of various food products. It helps to prevent the oxidation of films by protecting the properties of food such as odour, colour, flavour and the nutrient content. The incorporation of compounds such as essential oils (EOs) into the polymer matrix also contributes in modifying the barrier property. The gas transmission rate (GTR) is a measurement of different types of gases and it depends

upon the structure of the edible film [63]. The edible biodegradable films also act as a barrier to control the transport of moisture, gaseous components (oxygen and carbon dioxide), lipids and flavours in order to prevent the deterioration of the quality of the food and simultaneously increase the shelf life of the food products. The determination of barrier property of any edible film is done by two kinds of measurements including water vapour transfer rate and oxygen transfer rate.

15.3.2.1 Water Vapour Permeability Rate (WVPR)

The WVP works as a function of temperature and vapour pressure gradient. The WVP measures the diffusion through the surface of the film and helps in the estimation of barrier property. The coated food materials such as fruits and vegetables, due to their irregular shapes and sizes make it difficult for the determination of WVP. In order to overcome these issues, García et al. in his previously reported works developed a biological replica of coated sliced carrots, where the determination of surface-area calculations were taken into account for WVP measurements. The WVPR measurements are greatly dependent on the barrier thickness, since it affects the water vapour transport through the film matrix. In case of amylase films and coatings, a lower WVP values can be obtained due to the higher amylose content, dense matrix structure, and higher degree of crystallinity than those of standard corn starch. Similarly, the addition of sunflower oil into the starch film matrix reduce the WVP of films and coatings [62]. The low rate WVP of edible films helps in the prevention of dehydration of foods in terms of packaging and coatings. The hydrophilic fraction of the film and rate of permeability depending on its hydrophilic-lipophilic ratio controls the transport of water vapour. The EOs are known to reduce the WVP of polysaccharide-based edible films due to their hydrophobic nature. Although, fewer differences could be evidenced between ALG and EOs containing films for consisting low oil content. Further, films prepared from sage oil-EOs showed a prominent reduction in WVP compared to ALG films ($p < 0.05$). Also, lipid components used in the films enhances the water vapour barrier property [64]. The water vapour barrier properties for any biopolymer films decrease upon the inclusion of greater amount of plasticizers such as glycerol, water in case of hydrophilic coatings, etc. The humidity difference also serves as a reason for altered WVP, where the increased humidity difference in the films provide improved WVP rate [64].

The water vapour transmission rate (WVTR) through the film is described as:

$$\mathrm{WVTR} = m_1/A \tag{15.1}$$

$$\mathrm{WVP} = L * \mathrm{WVTR}/(\rho_i - \rho_a) \tag{15.2}$$

where, A (m^2) is the exposed film area, ρ_i (Pa) and ρ_a (Pa) are the vapour pressures of saturated air and with 33% RH, respectively at a temperature of 25 °C. L is the average film thickness (m), $m_1$is the slope of the curve from weight loss of the film versus time.

15.3.2.2 Oxygen Transmission Rate (OTR)

The oxygen permeability (OP) is an essential property of the edible films and coatings. It is a crucial parameter for keeping quality and physiological aspects of coated fruit products during storage. The OP is checked in case of films, rather than coated products. The oxygen and carbon-dioxide barrier of the film leads to a reduction in the respiration rate of the film. This is achieved by limiting exposure to surrounding oxygen, increase carbon dioxide content, which in turn provide delayed ripening and aging with extended storage life of coated fruits [62]. Rojas-Graü and colleagues (2007), reported the incorporation of antimicrobials agents (oregano, carvacrol and lemongrass oil) into ALG based edible films, where, the antimicrobial agents has less effectiveness to the OP of the ALG based edible films [65]. Also, it has been reported that the incorporation of EOs also increases the OP due to its hydrophobic character. McHugh et al. studied the integrated property for whey-protein edible films where they found that the presence of sorbitol is much more effective as a plasticizer than glycerol for the films which showed lower oxygen permabilities. Additionally, the protein films are considered as poor moisture barrier, mostly because of its hydrophilic nature but serves as a good barrier for oxygen and carbon-dioxide [66].

15.3.3 Mechanical Properties

The food packaging industries always put an effort towards protecting the packaged food from environmental issues and mechanical stresses. The mechanical properties of edible films and coatings are generally dependent on filler-matrix interactions, physical, chemical and temperature conditions which influence the film stability and flexibility. According to the ASTM D882-91 method, the mechanical properties of the films are characterized in terms of (a) deformation at break (extension at the moment of rupture, mm), (b) percent elongation at break (EAB) (deformation divided by initial probe length and multiplying by 100%), (c) tensile strength (TS) (force at rupture divided by film cross section, MPa) and (d) elastic modulus (slope of force-deformation curve, N/mm) [62]. The tensile properties of the edible films are dependent upon the film's mechanical resistance due to cohesion, relative proportion and preparation conditions, whereas, the EAB is related to the plasticity of the film. The edible film composites, particularly in case of incorporation of citral EO into the films revealed improved mechanical resistance with respect to the neat films, making it more feasible for food wrapping applications [63]. Additionally, various kinds of sustainable bionanostructured materials are used such as nanocellulose, nanochitosan, nanostrach and inorganic nanofiller materials to obtain improved packaging properties such as mechanical property [67] In the study of mgCNF on CS based edible coating, the mechanical properties related to this revealed remarkable improvement in the TS (57.86 ± 14 MPa) and Young's modulus (2348.52 ± 276 MPa) as compared to neat CS (6.27 ± 0.7 and

462.36 ± 64 MPa, respectively) [4]. Further, the puncture force (PF) is the maximum force required to break a film with the help of a penetrating tip, which describes the film rigidity. In this regards, the films which are made from nanoemulsions showed significant lower values of PF as compared to the ALG films (11.47 ± 1.05 N) [64]. The CS also proves as a partial replacement for methylcellulose (MC) in terms of better puncture resistance and economic benefit [62].

The TS and EAB of the packaging materials are calculated as:

$$TS = F_{max}/A \tag{15.3}$$

$$EAB = L/L_0 * 100 \tag{15.4}$$

where, F_{max} is the maximum load for breaking films (N), A is the cross-sectional area of the sample (thickness * width), L_o represents the initial gage length (50 mm) of the sample, L is the final length of the film before the moment of rupture.

15.3.4 Optical Properties

The colour and the optical properties for edible films are very important in terms of food packaging applications. The optical properties include transparency and colour coordinates as L^*(lightness), a^* (red-green) and b^* (yellow-blue) values among hot buffer and alkaline soluble solid fractions. The optical properties of the edible films help in beautifying the overall appearance of the packaged food product which in turn affects the consumer acceptance. The EO based edible films ($p < 0.05$) affected L*, a*, b* parameters and difference of color (DE*) in edible films. The L* showed higher values in case of lemongrass (LG-EO) and sago (SG-EO) nanoemulsions, whereas ALG and thyme (TH-EO) showed lower values. The a^* indicated negative values with green color which significantly reduced to 0.83 ± 0.05 in the edible films of TH-EO. The coordinate b^* showed positive values with yellow colour and the most positive value (6.9 ± 0.6) was observed in TH-EO films, thus pertaining that these films showed light greenish-yellowish tone [64]. The edible films are fabricated through solution casting processes showed improved optical properties, in terms of food packaging. In general, the transparency of the packaged food materials is determined in different regions in case of ultraviolet (200–400 nm) and visible (400–700 nm) ranges.

Film Transparency. The film transparency (T) is considered to be important property for food packaging films and coatings. The whey protein isolate showed highest transparency value of 1.07 ± 0.15%, which is greater than any of the polystyrene or blended films (<0.05). The pure MC, hydroxypropyl methylcellulose (HPMC), sodium ALG films showed higher percentage of transparency values as compared to low density polyethylene, high density polyethylene, and polypropylene (PP) films (<0.05), which are commonly used in case of food

packaging [68]. There are different food products which could be degraded by exposure to UV and visible range radiations. The percentage light transmission of the films is generally measured by using UV–Vis spectrophotometry. The % light transmission rate of the films is calculated by multiplying with the thickness of films (in cm) measured. In some of the food components such as proteins, lipids and fats, there may occur oxidation on exposure to light so reducing the transparency can also prove to be advantageous for packaging materials.

Color Property. The colour properties of the packaging materials in case of food products is measure generally, using coordinates including L, a*, b* and hue value. It is used to describe the quality, property and competence of the food products. Additionally, the colour parameters provide a safety tool for determining the product adulteration, the stability of pigment materials, the browning effects, etc. These factors are mostly affected by the incorporation of filler materials into the polymer matrix [4]. The colour parameters range from $L = 0$ (black) to $L = 100$ (white), −a (greenness) to +a (redness) and −b (blueness) to +b (yellowness). The total colour difference, ΔE is defined as [69]:

$$\Delta E = \sqrt{(L^* - L)^2 + (a^* - a)^2 + (b^* - b)^2} \tag{15.5}$$

and,

$$\text{YI (yellowness index)} = \frac{142.86\, b}{L} \tag{15.6}$$

$$\text{WI (whiteness index)} = 100 - \sqrt{(100 - L)^2 + a^2 + b^2} \tag{15.7}$$

where, L^*, a^*, and b^* are the standard colour parameter values and L, a and b are the colour parameter values for the sample.

15.3.5 Morphological Properties

The morphological properties of the food packaging materials are necessary to gather information about the size and shape of the framework of the polymer and the filler used for the edible films and coatings. It is generally characterized by FESEM analysis. This analysis also supports various other properties such as tensile and other physical properties. Sohail et al. (2006) investigated the morphological properties of edible casein films containing zein hydrolysate. The incorporation of wax into the casein films revealed similar smooth and uniform textures as in case without wax application. It ascribed towards the hydrophobicity of zein hydrolysate which is incorporated as a filler into the casein films [70]. The morphological analysis of CS-CNF and CS-mgCNF was carried out by FESEM analysis and the different kinds of morphological distributions were observed as a fiber like

dispersion and aligned particles (mgCNF) dispersion of nanofillers [4]. The FESEM studies in case of neat pea starch (PS) showed swollen starch granules structures and for neat peanut protein isolate (PPI) films showed presence of cavities and the blends of these with PPI at 40% level, revealed a flexible network type morphology of the edible films [71]. Thus, the morphology and percholation networks can be studied using FESEM micrographs.

15.3.6 Thermal Properties

The thermal property of edible film applications is also considered as one of the main attributes in wide utilization of developed edible film materials. The thermal property of the films is generally characterized by the differential scanning calorimetry technique (DSC) and thermogravimetric analysis (TGA). The DSC is a thermos analytical technique in which the heat difference is calculated between the sample and the reference. The TGA analysis details about the mass and composition of the edible films. In this technique, a sample is heated with different degradation temperature, where the weight fraction and change of mass are calculated. The analysis depends on the starting sample mass, the type and amount of NPs [6]. In the study of DSC analysis of the kefiran films with different glycerol contents showed the interaction between the polymer and the plasticizer which is necessary for food packaging applications [72]. The thermal stability of mgCNF improved considerably, where ∼17% of reduction in weight is observed, whereas the CNF degrades completely under the temperature range of 30–700 °C. The TGA analysis shows that there is an improvement in thermal stability for both CNF- and mgCNF-reinforced CS nanocoatings, where mgCNF provided more heat dimensional stability as compared to CNF- dispersed CS nanocoated films [4]. Yoo et al. (2011) studies the thermal properties of whey protein and polysaccharide edible films, where the thermal transitions of the biopolymers can be reviewed using DSC [68]. Martins et al. (2013) studied the synergistic effects between k-carrageenan (k-carr) and locust bean gum (LBG) edible films. The TGA curves depicted all events of k-carr/LBG films and found the films are stable up to 60 °C and a loss of 55% up to 319.2 °C occurs due to LBG thermal decomposition [73].

15.3.7 Physicochemical Property

The physiochemical properties of edible films and coatings include the measurement of water solubility, viscosity, moisture content, and stability of film-forming dispersion.

Water Solubility. The water solubility is an important parameter to be analysed in terms of possible applications of biopolymer edible films. The film solubility in water is defined as the ratio of water-soluble dry matter of film to that of the

dissolved after dipping in the distilled water. The percentage of the total soluble matter (% TSM) of the films is calculated using the below equation.

$$\%\text{TSM} = [(\text{Initial dry weight} - \text{Final dry weight})/\text{Initial dry weight}] \times 100 \quad (15.8)$$

Ghasemlou et al. (2011) found that the solubility of the films generally increases gradually with increased glycerol content. In case of glycerol-plasticized films, the addition of glycerol can diminish interactions between biopolymeric molecules, but, increase the solubility due to its hydrophilic nature, making the polymer more attracted towards water molecules [72]. Also, films developed from MC are completely soluble in water, whereas CS films provide lower water-solubility values. The composite of MC and CS provide reduced water-solubility values with increased CS concentration [62].

Viscosity. The viscosity measurement of the edible films is quite important in terms of food packaging applications. The spray coating process requires a low viscosity solution, whereas the immersion coating solution requires higher viscosity solution. In the case of nanoemulsions, viscosity is considered as one of the most relevant parameters since it showed a significant effect on EO loaded nanoemulsions' stability, which is based on the rheological study of the emulsion phases. The viscosity of pure sodium ALG solutions was found as 800 mPa s, whereas, EO type significantly ($p < 0.05$) affected viscosity of nanoemulsions (with lemon-grass EO, LG-EO incorporated sodium ALG solution has viscosity of 616 ± 62 mPa s). Since, EOs are complex in their mixing with different components, this might lead to different adsorption kinetics between ALG molecules and the oil droplets. Also, the high viscosity of nanoemulsions could affect the effectiveness of the droplets disruption because of the microfluidizer, which could lead to inclusion of sufficiently intense disruptive forces at the required pressure [64].

Moisture Content. It is defined as the weight of the moisture gained by the film per unit time (g/s). The knowledge of the relative importance of different available mechanisms controlling the moisture transfer through hygroscopic films is also very important for designing new edible films with improved and selective barrier properties. The hydrophobic nature of the films is also an important parameter to control the sensitivity of the films to moisture and it is commonly analysed by the contact angle measurements. If films are formed from raw polymeric ingredients, then it might be brittle even under low moisture conditions. So, plasticizers are used in order to increase the flexibility of the films and to reduce moisture sensitivity. In addition, a high amount of plasticizer may reduce the mechanical and barrier properties of the films. Thus, the ratio of polymer to plasticizer is important for determining the functional properties of the film. The analysis of moisture sorption is an indication of its storage stability in reduced moisture environments. The moisture content of most of the foods increases sigmoidally with respect to water, where the relationship is measured by a_w, which is the moisture sorption (or desorption) isotherm of the food. The moisture content plays an important role in order to reduce the exchange of water between the food and the environment [74].

Stability of Dispersion and its Rheological Property. The film-forming dispersions provide tailored property in the film structure, and improved film attributes. The SEM analysis plays an important role in film homogeneity, film structure, surface smoothness, and thickness. The surface of plasticized films (can be analysed by SEM) containing lipid molecules exhibited smooth surfaces and compact structure, which indicated a homogeneous dispersion of lipids within the film matrix [62]. Additionally, the drying time of films, plays a vital role in determining the arrangement of the components during the film-forming process of the edible films. In the study of magnetic cellulose nanofiber (mgCNF) dispersed CS-based edible nanocoating, the inclusion of filler material mgCNF provide the possible intercalation within the polymer matrix for increased interactions and better dispersion due to negligible agglomeration [4]. The film forming dispersions generally follows two mechanisms such as dry process and wet drying mechanism. In dry process, such as in extrusion, the polymers are heated above their glass transition temperature, Tg, under low water-content conditions. The edible film forming process generally follows the wet forming mechanism, where the polymers at first are dispersed in liquid phase and then dried. In this, the edible preformed films and coatings are formed by dipping, brushing or spraying. The rheological properties mostly depend on the design characteristics and processing conditions of film forming solutions or dispersion. Peressini et al. (2003) studied the rheological properties of edible film-forming dispersions containing corn starch, MC and glycerol using oscillatory and steady shear flow tests [75]. The combined effects of both the glycerol content and blending levels of MC with starch are evaluated in order to obtain the information relevant to the food coating. The film-forming dispersions depicted shear-thinning behaviour under steady state shear flow. The flow property evaluation can be carried out by the Herschel–Bulkley model (as shown below), in order to fit the flow data of dispersions with MC lower than 31%.

$$\tau = \tau o + K_{\gamma}^{\cdot n} \tag{15.9}$$

where,

τ(Pa) is the shear stress, $\gamma^{\cdot}(s^{-1})$ is the shear rate, τo is the apparent yield stress, K (Pa s^{-n}) and n (dimensionless)are the consistency and flow indexes, respectively.

Further, a systematic study of the rheological behaviour of the film-forming dispersions containing starch and MC have provide the effects of film formulations on the non-Newtonian behaviour and viscoelastic properties of the film-forming dispersions [75].The rheological properties of several emulsions are mainly associated with the characteristics of both the dispersed phase (volume concentration, distribution, size, shape and electrical charge of the particles), the continuous phase (viscosity, chemical composition, and concentration of electrolytes) and use of different types of surfactants and thickening agents. The use of microfluidization treatments in these emulsion appeared to be a suitable approach in the production of ALG based film-forming dispersions for targeted application [64].

15.4 Shelf Life Analysis of Food Products

As shown in Fig. 15.5, the shelf life analysis of food products is evaluated based on various properties such as physicochemical properties, respiration rates of fruits and vegetables, sensory evaluation, texture properties, microbiological study, color properties, texture properties, etc. Among available properties of food products, the sensory properties play a key role in the commercialization of any developed food products, as consumer acceptance is necessary for successful marketing of the product. However, the various food products undergo changes in nutritional quality during storage life, where the nutritional composition in food products vary from sources to sources. The fruit products with a fresh smell and having a proper size, consistency, and shape are more acceptable in comparison to other non-uniform and foul-smelling fruit products (which occurs due to environment degrading factors). In this regards, the food products should maintain the consistency, food property, and microbiologically safe for the entire product life. Additionally, the packaging materials in terms of primary and secondary packaging materials are used to carry the fruit products, where the packaging materials or food contact materials (FCMs) should be safe for food products. Additionally, the FCMs such as food manufacturing equipment, food packaging materials, food preparation/dining wares, and others are tested with different food simulants including acetic acid 3% v/v, ethanol 10% v/v, ethanol 50% v/v, vegetable oil, distilled water, and others to ensure safe consumption. Interestingly, the level of migration from FCMs to foodstuffs generally depends on several factors such as storage temperature, storage time, type of food products, type of packaging, etc., where, the migration of several components from the printing inks, varnishes, adhesives, inner bags, foodstuffs, and others may occur. In this regards, the fruits and vegetables, fish products, meat and meat products, dairy products, and others are analysed for various components to ensure safe storage and quality analysis. The materials and methods that are accompanied for analysis of shelf life of food products have been discussed in the following sections.

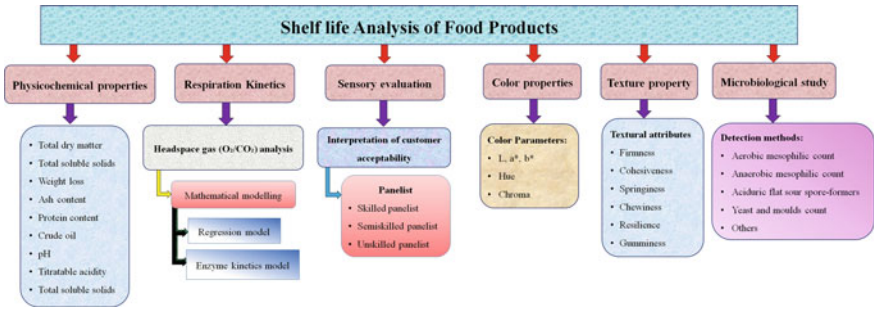

Fig. 15.5 Several property analysis of stored food products

15.4.1 Physicochemical Properties

The several physicochemical properties of food products include the analysis of moisture content, total dry matter, total soluble solids (TSS), weight loss analysis, and other properties (ash content, protein content, dietary fiber content, fat content, pH, titratable acidity ([TA], etc.). The nutritional composition of food products such as moisture content, ash, carbohydrate content, crude protein, and crude fiber is determined according to the standard methods of AOAC, 2010 [76] [**AOAC, 2010**]. The moisture content is determined following the gravimetric method, where an amount of 5 gm (W) is weighted and kept in an oven at 105 °C for 24 h, where the moisture content is determined from the percentage weight loss of the products. The dry matter of food products is generally calculated by measuring the weight difference of food products before and after drying (at 70 °C). The endpoint of after drying is selected till the constant weight of product is obtained. The pH of fruit products is determined using a pH meter. The pH of fruit products generally increases during storage due to ripening. Further, the TSS of fruit products is determined using a portable digital refractometer. The TSS content of fruit products increases during storage due to ripening. The TA of fruit products are determined by taking 250 g of well mixed juice, which is titrated against 0.1 M NaOH and the results are expressed as a percentage of malic acid. Additionally, the weight loss analysis of fruit products are measured by calculating the initial (weight at 0 days) and final (weights at sampling day) weights of the food products using a weighing balance [4, 77, 78]. The percentage weight loss of the stored food products is generally measured using the below Eq. (15.10):

$$Weight\ loss\ (\%) = \frac{m_0 - m_s}{m_0} \times 100 \tag{15.10}$$

where, m_0 and m_s are the sample weight at 0 day and sampling day, respectively.

15.4.2 Study on Respiration Kinetics

The fruits and vegetables continue respiring even after getting detached from the mother plant. The respiration in living plant products occur continuously by consuming O_2 from the surrounding and releasing CO_2 to the environment [79]. The respiration rates of plant materials have an inverse relation with the shelf life of plant materials, where increased respiration rates decrease the shelf life of commodities [80]. The respiration of living food commodities is considered as a crucial factor responsible for postharvest wastes of perishable fruits and vegetables. Further, the design of modified atmospheric packaging (MAP) and controlled atmospheric packaging (CAP) of food products depend on the respiration rate of fruit products. However, the respiration of food products is influenced by the

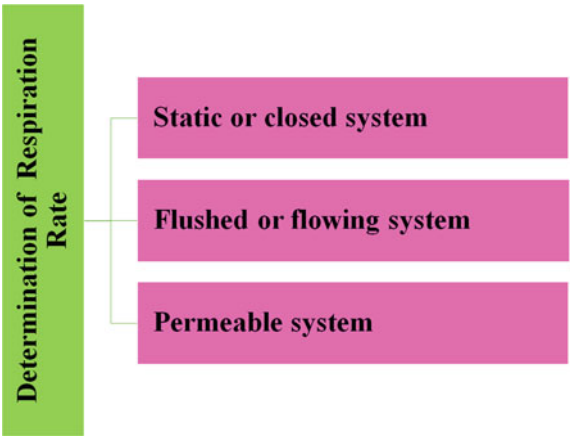

Fig. 15.6 Available methods for respiration rate measurement

storage temperature, gaseous composition, storage time, commodity type, etc. Besides respiration, respiration quotient is another factor associated with respiration of commodities, which is defined as the ratio of produced CO_2 to consumed O_2 during respiration cycles. However, as represented in Fig. 15.6, the common methods of measuring the respiration rates include static or closed system, flushed or flowing system, and permeable system [81].

Closed or Static Method for Respiration Rate Measurement. The closed or static system is a non-destructive method, time consuming, and labor consuming process, however, it can test different gaseous combinations, and the method is suitable for low respiring products [81]. In a static or closed system, the respiration study is generally conducted at various storage temperatures for a various time period (storage time depends on the storage temperatures). For this kind of respiration rate measurements, a specific amount of fruit products is stored in airtight close chamber, with ambient air as the initial gas composition as shown in Fig. 15.7. The gas chamber should have some headspace after loading of selected commodity for measuring the respiration rates. The practice of applying Vaseline white between the cover and the open top side of the container to avoid any gas leakage. Further, there is available gas septum on the top of the airtight chamber, where syringe is inserted to obtain the data set of gas concentrations in the headspace of gas chamber. A gas analyzer is generally used to analyze the O_2/CO_2 gas concentration in the headspace of the chamber. Besides, the gas chromatographs or O_2 probes are also used to determine the respiration rate of fruit products. In the closed system method, there is a need to estimate the free/gaseous volume of the closed chamber, which is difficult to estimate the same. The close chamber is generally kept inside the incubator to maintain the storage temperature of the selected food products. Additionally, the use of temperature sensors also helps to indicate the temperature of the airtight chamber.

The respiration rate of fruits and vegetables can be determined by the ratio of gas exchange amount to the amount of sample taken and storage periods. The various

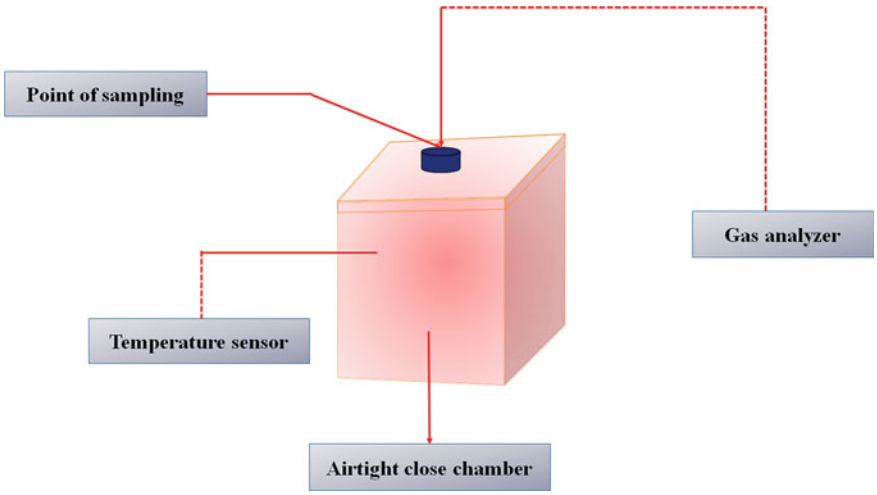

Fig. 15.7 Determination of respiration rate of fresh fruit products using airtight close chamber

dataset is collected and respiration rate in terms of O_2 and CO_2 gases are determined using the Eqs. (15.11) and (15.12).

$$\mathrm{RR}_{\mathrm{O}_2} = \frac{\left(\mathrm{GC}^{i}_{\mathrm{O}_2} - \mathrm{GC}^{f}_{\mathrm{O}_2}\right) \times V_f}{100 \times W \times (\Delta t)} \tag{15.11}$$

$$\mathrm{RR}_{\mathrm{CO}_2} = \frac{\left(\mathrm{GC}^{f}_{\mathrm{CO}_2} - \mathrm{GC}^{i}_{\mathrm{CO}_2}\right) \times V_f}{100 \times W \times (\Delta t)} \tag{15.12}$$

The linearization of Eqs. (15.11) and (15.12) are given in the Eqs. (15.13) and (15.14).

$$\mathrm{GC}^{f}_{\mathrm{O}_2} = \mathrm{GC}^{i}_{\mathrm{O}_2} + \frac{\mathrm{RR}_{\mathrm{O}_2} \times W}{V_f}(t - t_i) \times 100 \tag{15.13}$$

$$\mathrm{GC}^{f}_{\mathrm{CO}_2} = \mathrm{GC}^{i}_{\mathrm{CO}_2} + \frac{\mathrm{RR}_{\mathrm{CO}_2} \times W}{V_f}(t - t_i) \times 100 \tag{15.14}$$

where, $\mathrm{RR}_{\mathrm{O}_2}$ (ml $\mathrm{kg}^{-1}\mathrm{h}^{-1}$) and $\mathrm{RR}_{\mathrm{CO}_2}$ (ml $\mathrm{kg}^{-1}\mathrm{h}^{-1}$) are the respiration rates of O_2 and CO_2 gases, respectively; V_f (mL) is the free headspace volume of the jar; W (kg) is recognized as the sample weight taken for the study; $\Delta t = t - t_i(h)$ is the storage time between two consecutive readings; $GC^{i}_{O_2}$ is the initial O_2 concentration, cm^3/cm^3 of space; $GC^{f}_{O_2}$ is the O_2 concentration at time t, $\mathrm{cm}^3/\mathrm{cm}^3$ of space; $GC^{f}_{CO_2}$ is the CO_2 concentration at time t, $\mathrm{cm}^3/\mathrm{cm}^3$ of space; and $GC^{i}_{CO_2}$ is the initial CO_2 concentration, $\mathrm{cm}^3/\mathrm{cm}^3$ of space.

Mathematical Modelling of Respiration Rate of Food Products. The mathematical modelling of respiration rate of fruit products can be studied based on enzyme kinetics and the Arrhenius equation as detailed in this section [79]. The several research reports based on the respiration study and mathematical modelling of several fruit products are available such as banana [82, 83], tomato [84], litchi [85], green mature mango [80], fig [86], bhimkol [87], apple [88], fresh cut pineapple [89], guava [90], blueberry [91], etc. The above mentioned equations are utilized to determine the respiration rates of specific food products in terms of O_2 and CO_2, which are further used for the mathematical modelling of respiration rates such as regression function model and enzyme kinetics model. The mathematical models are developed to correlate the respiration rate of fruit products with different storage parameters including storage temperature, and gaseous composition. In this regards, Mahajan & Goswami have done the enzyme kinetics based mathematical modelling of apple, where the respiration rates of apple in terms of O_2 and CO_2 follow uncompetitive inhibitions [79]. Further, a detail of the available regression function model and enzyme kinetics model for respiration kinetics study have been described below.

Regression Model. The regression function is used to fit the gas concentration dataset of commodities versus storage time, where the respiration rates of the commodities are determined from the first order derivatives of the regression function [82]. The respiratory behaviour of perishable food products is studied using regression function model, where the temperature dependence of model co-efficient can be determined by curve fitting method. The respiration data sets are used to fit gaseous concentrations at various time periods using the Eqs. (15.15) and (15.16).

$$GC_{O_2}^{f} = GC_{O_2}^{i} - \left[\frac{t}{(at+b)}\right] \tag{15.15}$$

$$GC_{CO_2}^{f} = GC_{CO_2}^{i} - \left[\frac{t}{(at+b)}\right] \tag{15.16}$$

where, a, and b are the regression coefficients. The first order derivatives of Eqs. (15.15) and (15.16) are represented in Eqs. (15.17) and (15.18) and can be used to measure the change in gaseous concentrations with storage time.

$$\frac{dGC_{O_2}}{dt} = at(at+b)^{-2} - (at+b)^{-1} \tag{15.17}$$

$$\frac{dGC_{CO_2}}{dt} = -at(at+b)^{-2} + (at+b)^{-1} \tag{15.18}$$

where, $\frac{dGC_{O_2}}{dt}$ and $\frac{dGC_{CO_2}}{dt}$ are the first order derivatives of gaseous concentrations in terms of O_2 and CO_2 gasses, respectively.

Enzyme Kinetics Model. The enzyme kinetics model is based on the principles of enzyme kinetics for the respiration rate predictions of fresh produces [82]. The enzyme kinetics model generally follows uncompetitive inhibitions. As represented in Eqs. (15.19) and (15.20), the model parameters are V_m, K_m, and K_i for O_2 consumption rate and CO_2 evolution rates.

$$\mathrm{RR}_{\mathrm{O}_2} = \frac{V_{mo}\mathrm{GC}_{\mathrm{O}_2}}{K_{mo} + \left[1 + \frac{\mathrm{GC}_{\mathrm{CO}_2}}{K_{io}}\right]\mathrm{GC}_{\mathrm{O}_2}} \tag{15.19}$$

$$\mathrm{RR}_{\mathrm{CO}_2} = \frac{V_{mo}\mathrm{GC}_{\mathrm{O}_2}}{K_{mo} + \left[1 + \frac{\mathrm{GC}_{\mathrm{CO}_2}}{K_{io}}\right]\mathrm{GC}_{\mathrm{O}_2}} \tag{15.20}$$

where, V_m (ml $kg^{-1}h^{-1}$)) is the maximum respiration rate; K_m is the dissociation constant (% O_2); K_i is the inhibition constant (%CO_2). Further, the Arrhenius relationship, which is a function of temperature, is chosen to describe the enzyme kinetics model of fresh produces. The parameters of enzyme kinetics model are determined using Arrhenius relations as represented in Eqs. (15.21) and (15.22).

$$\mathrm{RR}_{\mathrm{O}_{2,m}} = \mathrm{RR}_{\mathrm{O}_{2,p}} \times e^{\left[\left(-E_{a,\mathrm{O}_2}/R\right)\left(\frac{1}{T}-\frac{1}{T_r}\right)\right]} \tag{15.21}$$

$$\mathrm{RR}_{\mathrm{CO}_{2,m}} = \mathrm{RR}_{\mathrm{CO}_{2,p}} \times \mathrm{e}^{\left[\left(-E_{a,\mathrm{CO}_2}/R\right)\left(\frac{1}{T}-\frac{1}{T_r}\right)\right]} \tag{15.22}$$

$\mathrm{RR}_{\mathrm{O}_{2,m}}$ is model parameter of Michaelis-Menten equation; $\mathrm{RR}_{\mathrm{O}_{2,p}}$ is respiration pre-exponential factor;$\mathrm{RR}_{\mathrm{CO}_{2,m}}$ is model parameter of Michaelis-Menten equation; $\mathrm{RR}_{\mathrm{CO}_{2,p}}$ is respiration pre-exponential factor; E_{a,O_2} activation energy, kJ g^{-1} mol^{-1}; E_{a,CO_2} activation energy, kJ g^{-1} mol^{-1}; R is the universal gas constant, 8.314 kJ g^{-1} mol^{-1} K^{-1}; T is recognized as the storage temperature, K; T_r is the reference temperature, K. The linearized form of the above Eqs. (15.12) and (15.23) are shown in Eqs. (15.24) and (15.25).

$$\mathrm{In}\ \mathrm{RR}_{\mathrm{O}_{2,m}} = -\frac{E_{a,\mathrm{O}_2}}{R}\left(\frac{1}{T} - \frac{1}{T_r}\right) + \mathrm{In}\ \mathrm{RR}_{\mathrm{O}_{2,P}} \tag{15.23}$$

$$\mathrm{In}\ \mathrm{RR}_{\mathrm{CO}_{2,m}} = -\frac{E_{a,\mathrm{CO}_2}}{R}\left(\frac{1}{T} - \frac{1}{T_r}\right) + \mathrm{In}\ \mathrm{RR}_{\mathrm{CO}_{2,P}} \tag{15.24}$$

Additionally, the Eq. 15.25 is used to study the temperature dependence of model parameters of Michaelis- Menten equation.

$$R_m = R_P \exp\left[-\frac{E_a}{RT_{abs}}\right] \tag{15.25}$$

R_m is the model parametric co-efficient for Michaelis-Menten equation; R_p is the pre-exponential frequency factor; T_{abs} is the absolute temperature, K

15.4.3 Sensory Evaluation

The sensory evaluation of a product involves the analysis and interpretation of the customer acceptability of a product using the human senses. The sensory analysis is applicable for executing experimental design and statistical analysis for the evaluation of consumer acceptance for a product. The customer acceptance of a product involves the smell, taste, sight, touch and others of the products. This sensory evaluation is generally done by skilled, semi-skilled and unskilled persons and the evaluation can be classified into three sub-sections such as analytical testing, affective testing, and perception as represented in Fig. 15.8. The analytical method of sensory evaluation includes the difference and descriptive analysis. The analysis of a difference test details/measures whether a product difference is acceptable from the existing product or not. On the otherhand, the affective method of sensory evaluation includes the hedonic and preference test, where the use of hedonic test measures the degree of liking of products. The hedonic scale can detail which product is most liked among the various products. The best timings for sensory testing are 10 AM–12 noon and 3 PM–5 PM.

Additionally, as represented in Fig. 15.9, the several types of sensory testing are difference test (Paired comparison test, Duo-Trio test, Triangle test), rating test (ranking test, single sample test, two-sample difference test, multiple sample difference test, Hedonic rating test, Numerical scoring test, composite scoring test), sensitivity test (Sensitivity threshold test/dilution test) and descriptive test. The paired comparison test includes the comparison of two different samples of food product based on one attribute (such as sensory evaluation for checking the

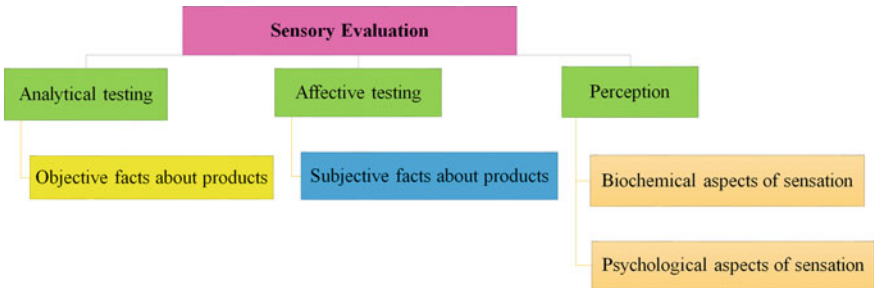

Fig. 15.8 Classification of sensory evaluation for food product testing

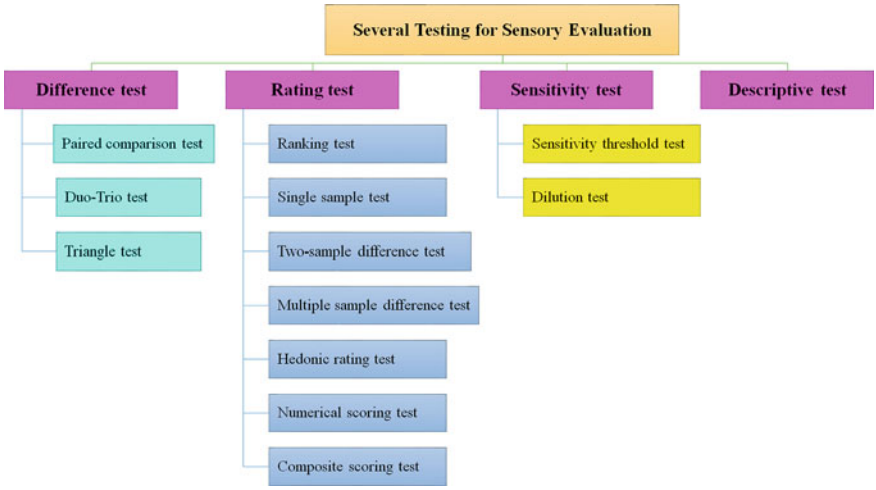

Fig. 15.9 Several Types of Sensory evaluation testing

smoothness of a sample). The duo-trio test includes the testing of three samples, where two samples are identical and one of the identical samples is taken as the control one. The panelist is supposed to find the identical sample (control) from the remaining two samples. In a triangle test, three samples are arranged in a triangle, where two of the three samples are identical. In this analysis, the panelist is asked to find the different one from the three samples. If the samples are named as "a" and "b", then the combinations of the samples arranged in a triangle are attained as either "aab" and "bba".

Moreover, the ranking test is a type of rating test, where several samples are given to the panelist with only code numbers and the panelist are asked to rank the samples based on a single attribute of a product. In the single sample test, the presence of particular quality attributes or the intensity of a quality attribute is determined by the panelist. For example, to detect the intensity (strong/moderate/strong) of off-flavor of a product and state the reason for off-flavor such as off-odor, off-taste, etc. The hedonic test based sensory evaluation is based on the 5-point (1: Dislike very much to 5: Like very much) or 9-point scale (1: Dislike very much to 9: Like very much) based testing, where the panelist put the remarks for taste, odor, color, texture, flavor, appearance. and overall acceptability of the product. Moreover, the Hedonic scale based on 9 scores is generally used for ranking food products and the scores provide the comment on the products, where 1: dislike extremely; 2: dislike very much; 3: dislike moderately; 4: dislike slightly; 5: Neither like or dislike; 6: Like slightly: 7: Like Moderately; 8: Like Very Much: 9: Like extremely. The sensory analysis of food products is generally evaluated for several attributes such as color, flavor, texture, taste, overall acceptability, and others using

Hedonic scale to find the most suitable and acceptable product among available. In this way, the sensory evaluation of food products is done to perceive, describe, and quantify the customer acceptability before commercialization.

15.4.4 Texture Property

The textural properties of food products are considered as the physical properties of food products, resulting from the macro/micro-structural properties of several food components. As discussed in the earlier section, the textural properties of food products can be analyzed and interpreted by panelist. However, the instrumentation methods of texture analysis are getting much interest due to several advantages such as rapid, economic, ease of standardization, etc. The texture properties of solid, semi-solid and liquid products are measured using the Texture analyzer instruments. The texture analysis of food products is executed via applying controlled forces (tensile/compressive forces) to the food products and the responses of the applied forces are obtained in the form of deformations, forces and time. The food texture is a very critical factor in food products to analyze the quality of food products for its overall acceptability. Among the several textural properties, firmness or hardness is one of the most essential properties for food products for determining the food quality. The firmness is a key parameter for fruits and vegetables. On the otherhand, crunchy food products should maintain the required crispiness for consumer acceptance. The other textural attributes are cohesiveness, adhesiveness, springiness, etc. The attributes for texture are moistness, oiliness, flakiness, dryness, crunchiness, etc. However, the textural attributes of food products include several characteristics such as (i) Mechanical characteristics: Primary parameters (hardness, cohesiveness, elasticity, viscosity, adhesiveness), secondary parameters (brittleness, chewiness, gumminess); (ii) Geometrical characteristics: Particle size and shape, particle shape and orientations; (iii) other characteristics: MC, fat content, greasiness, etc. [92, 93]. In this regards, the several probes for texture analysis of food products include the use of cylinder, cone, ball, blade, wire, plate, knife, etc., where the selection of probes depends on the selected food product.

Texture Profile Analysis. Additionally, the texture profile analysis (TPA) is the measurement of food texture where the spatial textural events of samples are monitored and recorded. The mechanical measurements of TPA of food products are classified into destructive and non-destructive methods, where the destructive methods include the testing such as puncture and penetration tests, three-point bending test, single-edge notched bend test, etc., whereas the non-destructive methods include impact response, quasi-static force-deformation, bioyield detection, etc. In non-destruction method of texture measurement for TPA analysis, there is no visible damages are obtained. As represented in Fig. 15.10, the texture modeling of food products includes first order reaction/kinetic model,

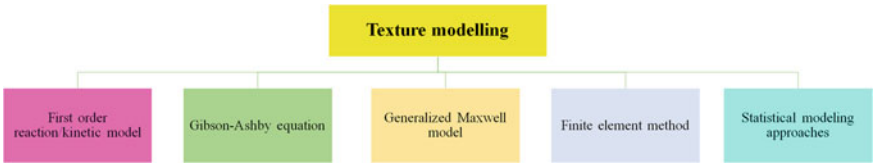

Fig. 15.10 Several Texture modelling of food products

Gibson-Ashby equation, Generalized Maxwell model, Finite element method (FEM), statistical modelling approaches, etc. [94]. Additionally, a model for mouth behavior can also be utilized to mimic the chewing behavior of food products [95]. The textural characteristics of food products including hardness, adhesiveness, springiness, cohesiveness, resilience, gumminess, chewiness and others can be analyzed using TPA to control the quality of the food products [96]. Moreover, the texture measurement for objective evaluation is classified into three types: fundamental, empirical, and imitative [97]. In this way, the textural attributes of stored food products with and without edible food packaging (films/coatings) are analyzed for customer acceptability and to maintain food texture.

15.4.5 Migration Study for Packaging Application

The NPs are widely utilized in the fabrication of composite based food packaging materials for obtaining the tailored-made properties. However, the NPs used in the packaging materials should have the migration values within the permissible limits. Thus, risk assessment of NPs and potential migration assays are required for maintaining the safety of the food products [98]. As discussed in earlier chapters, the nanotechnology has received a great deal of interest in developing FCMs, where the FCMs is classified into various sectors such as improved packaging properties with NPs reinforcements, active packaging due to reinforcement of active NPs, intelligent packaging with nanosensors, biocomposite based packaging materials, etc. Additionally, all packaging materials generally have the problems of migration of several chemical substances from FCMs into food stuffs such as food additives, monomers, food residues, etc. [99]. The migration study in food packaging is generally defined as a mass transfer phenomenon, where low molecular weight components are firstly diffused into the food products, and the mechanism of migration behavior of food components can be described by Fick's second law. Thus, in migration testing, the release of substances from the packaging materials into the food products or to the food simulants are determined. Further, the migration models are generally developed based on Fick's second law, where the diffusion coefficients are estimated for the modelling of partition migration [100]. The migration tests are conducted following the rules and regulations of Commission Regulation EU No. 10/2011 [101]. For the determination of overall

migration, a specimen/film having area of 1 dm^2 of contact area per 100 mL of simulants are stored for 10 days at 40 °C. According to the European Regulation, the migration study is generally studied using overall migration tests and specific migration tests [102].

Interestingly, the migration of several compounds in food products occurs following several steps such as (1) the diffusion of chemical compounds due to Brownian movement such as unreacted monomers, monomers developed from packaging materials due to adverse conditions. However, the generation of chemical compounds during storage of food products or heating depends on several factors such as type of packaging materials, temperature, time period, and others. (2) desorption of the absorbed compounds from the polymeric surface; (3) solvation or migration of the compounds to food products from food-plastic interface, where solvation of compounds occurs when the migrants have the better solubility in food products than in FCMs; and (4) dispersion into bulk food materials. The migration of several plastic compounds may held by various ways such as (1) diffusion mechanism (direct contact migration): The compounds of packaging materials diffused from the packaging layer to the FCMs; (2) Gas phase migration is considered as indirect contact migration where the volatile compounds are generally generated due to high temperature exposure and can migrate from the packaging materials to the FCMs; and (3) Set off migration is generally caused due to migration of compounds during manufacturing and storage. Additionally, in packaging materials, the migration can occur through several ways such as penetration migration, contact/set off migration, evaporation migration, and temperature gradient migration. As shown in Fig. 15.11a, the penetration migration in packaging films occurs from printed side to the unprinted side (FCMs) through the substrate. The contact/set off migration (Fig. 15.11b) occurs from the printed side to

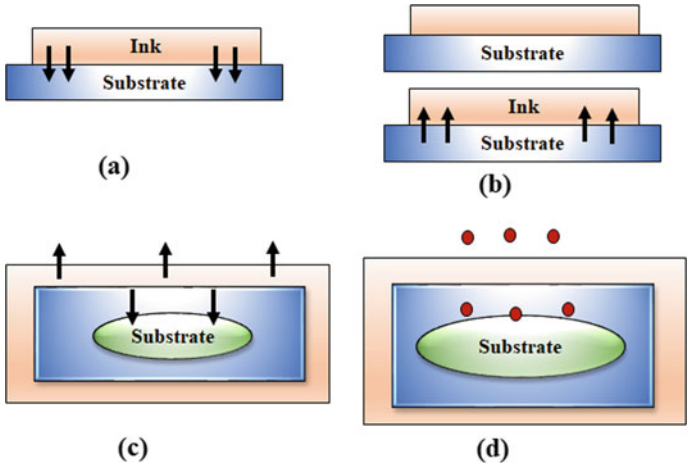

Fig. 15.11 General mechanisms of migration (a) Penetration migration, (b) Contact/Set off migration, (c) Evaporation migration, and (d) Temperature gradient migration

the unprinted side of the substrate, when remains in contact with each other. The evaporation migration (as shown in Fig. 15.11c) held due to the evaporation of several volatile compounds from the packaging materials during heating such as microwave heating of food products with the containers. The temperature gradient migration (Fig. 15.11d) causes due to the raising temperature such as sterilization. Further, the use of functional barrier may decrease the migration of packaging components to food simulating liquids [103].

Several Migrating Components from Food Contact Materials. The migrating components to food products include isopropylthioxanthone, epoxydised soy bean oil, diethylhexyl phthalate, primary aromatic amines, plasticizers, additives (plasticizers, coloring agents, heat stabilizers), etc. The potential migrants in food products are antimicrobials, colorants, UV absorbers, light stabilizers, plasticizers, anti-fogging additives, and others. The contaminants such as plasticizers, heavy metals, polyaromatic hydrocarbons, fluorescent whitening agents, residual solvents, etc. are generally analyzed for recycled paper and boardwhen used as a packaging materials [104]. The volatile compounds in pellets and packaging materials for food products are 2-Methyl-1-propene, 2-Propanone, dichloromethane, cyclohexane, ethylbenzene, xylene, styrene, decane, dodecane, heptane, 3-methyl pentene, cyclohexanone, tetradecane, pentadecane, octadecane, etc. [105]. Several plastic containers are used to carry food products in microwave ovens, where volatile compounds can release and migration of the compounds can occur from container to food products [105]. The several plastic containers used for microwave heating are polycarbonate, PP, PP-copolymer, and others. The plastic containers are not inert and diffusion of different plastic components held when food products are packed within it. The plastic components get diffused from the plastic to the food products, where increase in temperature may increase the migration of plastic compounds. In plastic based packaging, the monomers such as styrene, vinyl chloride, isocyanate, caprolactam, and others can create adverse health effect due to carcinogenic nature if get diffused or leached out to food products.

Food Simulants for Migration Testing. The food simulants for migration testing include water, acidic water (mimic acidic foods), 15% ethanol (mimic alcoholic beverages), and rectified olive oil (mimic fatty foods) [106]. Tenax® is another known dry food simulant, which consists of granules of modified polyphenylene oxide [107]. A research reports the study on migration of adhesives into Tenax®, where 57% of total compounds (55 different compounds) are found to migrate in the selected food simulants [107]. Further, porapak is also found to use as a solid food simulant for paper and board packaging and further, porapak is having stable property even at high temperature in comparison to Tenax [108]. For paper and board based packaging, several food products including pasta, milk powder, dry soup, flour and bakery products, icing sugar and others has been tested for migration study [104]. The perfluorochemicals are also used to prepare FCM such as polytetrafluoroethylene, and the development of this kind of materials involve the use of perfluorooctane, sulfonate, perfluorooctanic acid, which are biopersistent in nature and can cause several health issues [103].

The use of nanoclay to develop food packaging application is found to provide very low migration value into food products in comparison to other nanomaterials using food simulants such as 10% ethanol and 3% acetic acid and storage conditions (1) 40°C for 10 days, and (2) 70 °C for 2 h [109]. Further, a study shows that the level of migration into pork meat products (packaged in low density polyethylene films and storage condition: 10 days and 25 °C) increase with increased storage temperature and fat content. Additionally, the use of nanomaterials such as silver NPs for developing biocomposite based packaging is dependent on the migration of nanomaterials from FCM into food products for safety purpose [110]. The migration analysis is time consuming and required specific conditions to study the behavior of packaging components. The detection of chemical substances that releases from plastic substances due to migration can be detected using a mass spectrometry such as High resolution mass spectrometry with enhanced accuracy [111]. In this regards, a report suggests the detection of various compounds from vacuum packed meat samples using a mass-spectrometry based instrumentations. Thus, the migration testing of packaging materials are essential to avoid the adverse health effect which may be caused by the several packaging compounds.

15.4.6 Other Properties

Besides, the above mentioned properties, the microbiological study to test the microbial growth in edible coated or stored food products are undergone. In this regards, the mesophilic and psychrophilic counts are determined during the storage life to test the effectiveness of edible coating and films in inhibiting or reducing the microbial growth. Moreover, other studies such as color properties, food composition are also determined to check the quality of stored food products.

15.5 Conclusions

The nanoscience and nanotechnology have played a vital role in the upliftment of the usage of the food packaging materials across the globe. The food, which is one of our basic needs of life, need to be consumed in a healthy manner. The developments of nanomaterials have paved a path to introduce essential nutrients towards healthier and safer consumption of food. The introduction of biodegradable and sustainable polymer edible films into this, would not only protect the food products from outside but also can be consumed along with the food. The incorporation of nano-biomaterials onto the food packaging can improve the shelf-life and quality of the food. The edible films that are introduced can be easily accepted by the cells of the body because of their various surface and size related properties. The developed biobased nanomaterials for edible food packaging are characterized by different characterization techniques that are discussed which can give us a greater idea of

different types of biomaterials used and their properties. The natural based biopolymers when incorporated with nano-biomaterials not only improves its surface properties but also mechanical properties and thermal properties to withstand various temperature conditions. Therefore, the introduction of the various biomaterials and their characterization helps in understanding and preventing the food from damage and also minimise the hazard from disposal of the packaging products. The sensory properties are considered as the most crucial element for attaining the consumer acceptability. The sensory properties of food products are taste, smell, appearance, texture, sound, mouthfeel and others, which can be well assayed by sensory evaluation process. The polymer based packaging materials developed through incorporating filler materials, cross linking agents, compatibilizers plasticizers and others, where some components or filler materials of packaging materials which are unable to react with matrix materials have a tendency to get trapped within the matrix materials. The trapped materials have a tendency to migrate from the packaging materials when attained a change in storage condition or get exposure to a similar kind of materials. However, the filler materials or other agents are generally incorporated in a small amount and the migration of the components should be within the permissible limits. Thus, the migratory components need to be controlled and regulated properly to avoid migration, and the migration of FCM to food products is found to obey the Fick's laws of diffusion. The migration of packaging components from FCM to food products generally depends on several factors such as nature of FCM, physical and chemical properties of food components, storage temperature, contact area, used adhesives for sealing the packaging materials, types of food products, etc.

Bibliography

1. Kriparamanan R, Aswath P, Zhou A, Tang L, Nguyen KT (2006) Nanotopography: cellular responses to nanostructured materials. J Nanosci Nanotechnol 6:1905–1919. https://doi.org/10.1166/jnn.2006.330
2. Gleiter H (2000) Nanostructured materials: basic concepts and microstructure. Acta Mater 48:1–29. https://doi.org/10.1016/S1359-6454(99)00285-2
3. Pathakoti K, Manubolu M, Hwang HM (2017) Nanostructures: Current uses and future applications in food science. J Food Drug Anal 25:245–253. https://doi.org/10.1016/j.jfda.2017.02.004
4. Ghosh T, Teramoto Y, Katiyar V (2019) Influence of nontoxic magnetic cellulose nanofibers on chitosan based edible nanocoating: a candidate for improved mechanical, thermal, optical, and texture properties. J Agric Food Chem 67:4289–4299. https://doi.org/10.1021/acs.jafc.8b05905
5. Sharma S, Jaiswal S, Duffy B, Jaiswal AK (2019) Nanostructured materials for food applications: spectroscopy, microscopy and physical properties. Bioeng 6:26. https://doi.org/10.3390/bioengineering6010026
6. Mourdikoudis S, Pallares RM, Thanh NT (2018) Characterization techniques for nanoparticles: comparison and complementarity upon studying nanoparticle properties. Nanoscale 10:12871–12934. https://doi.org/10.1039/C8NR02278J

7. Upadhyay S, Parekh K, Pandey B (2016) Influence of crystallite size on the magnetic properties of Fe_3O_4 nanoparticles. J Alloys Compd 678:478–485. https://doi.org/10.1016/j.jallcom.2016.03.279
8. Yan W, Petkov V, Mahurin SM, Overbury SH, Dai S (2005) Powder XRD analysis and catalysis characterization of ultra-small gold nanoparticles deposited on titania-modified SBA-15. Catal Commun 6:404–408. https://doi.org/10.1016/j.catcom.2005.04.004
9. Li W, Zamani R, Rivera Gil P, Pelaz B, Ibáñez M, Cadavid D, Cabot A (2013) CuTe nanocrystals: shape and size control, plasmonic properties, and use as SERS probes and photothermal agents. J Am Chem Soc 135:7098–7101. https://doi.org/10.1021/ja401428e
10. Koningsberger DC, Prins R (1988) X-ray absorption: principles, applications, techniques of EXAFS, SEXAFS, and XANES
11. Heinz M, Srabionyan VV, Bugaev AL, Pryadchenko VV, Ishenko EV, Avakyan LA, Dubiel M (2016) Formation of silver nanoparticles in silicate glass using excimer laser radiation: Structural characterization by HRTEM, XRD, EXAFS and optical absorption spectra. J Alloys Compd 681:307–315. https://doi.org/10.1016/j.jallcom.2016.04.214
12. Pugsley AJ, Bull CL, Sella A, Sankar G, McMillan PF (2011) XAS/EXAFS studies of Ge nanoparticles produced by reaction between Mg_2Ge and $GeCl_4$. J Solid State Chem 184:2345–2352. https://doi.org/10.1016/j.jssc.2011.06.020
13. Chen X, Cai Q, Wang W, Mo G, Jiang L, Zhang K, Wu Z (2008) Formation of Ge-S Bonds from AOT-Coated GeO_2 Nanoparticles at High Temperature: An in Situ Heating EXAFS Investigation. Chem Mater 20:2757–2762. https://doi.org/10.1021/cm703368u
14. Ramallo-Lopez JM, Giovanetti L, Craievich AF, Vicentin FC, Marín-Almazo M, José-Yacaman M, Requejo FG (2007) XAFS, SAXS and HREM characterization of Pd nanoparticles capped with n-alkyl thiol molecules. Physica B 389:150–154. https://doi.org/10.1016/j.physb.2006.07.044
15. Pizarro SA, Glatzel P, Visser H, Robblee JH, Christou G, Bergmann U, Yachandra VK (2004) Mn oxidation states in tri-and tetra-nuclear Mn compounds structurally relevant to photosystem II: Mn K-edge X-ray absorption and Kβ X-ray emission spectroscopy studies. Phys Chem 6:4864–4870. https://doi.org/10.1039/B407513G
16. Rehr JJ, Albers RC (2000) Theoretical approaches to x-ray absorption fine structure. Rev Mod Phys 72:621. https://doi.org/10.1103/RevModPhys.72.621
17. Yano J, Yachandra VK (2009) X-ray absorption spectroscopy. Photosynth Res 102: 241. https://link.springer.com/article/10.1007/s11120-009-9473-8
18. Cinco RM, McFarlane Holman KL, Robblee JH, Yano J, Pizarro SA, Bellacchio E, Yachandra VK (2002) Calcium EXAFS establishes the Mn-Ca cluster in the oxygen-evolving complex of photosystem II. Biochemistry 41:12928–12933. https://doi.org/10.1021/bi026569p
19. Sharma A, Varshney M, Park J, Ha TK, Chae KH, Shin HJ (2015) XANES, EXAFS and photocatalytic investigations on copper oxide nanoparticles and nanocomposites. RSC Adv 5:21762–21771. https://doi.org/10.1039/C4RA16217J
20. Wang W, Chen X, Cai Q, Mo G, Jiang LS, Zhang K, Pan W (2008) In situ SAXS study on size changes of platinum nanoparticles with temperature. EUR PHYS J B 65: 57–64. https://link.springer.com/article/10.1140/epjb/e2008-00322-7
21. Singh M, Sinha I, Singh AK, Mandal RK (2011) Correlating SAXS analysis with LSPR behavior: poly (vinyl alcohol)-stabilized Ag nanoparticles. J Nanopart Res 13: 4387–4394. https://link.springer.com/article/10.1007/s11051-011-0388-x
22. Bulavin L, Kutsevol N, Chumachenko V, Soloviov D, Kuklin A, Marynin A (2016) SAXS combined with UV–V is spectroscopy and QELS: accurate characterization of silver sols synthesized in polymer matrices. Nanoscale Res Lett 11: 35. https://link.springer.com/article/10.1186/s11671-016-1230-2
23. Liang YC, Juan YW, Lu KT, Jeng US, Chen SA, Chuang WT, Sheu HS (2012) Formation process of mesostructured PtRu nanoparticles electrodeposited on a microemulsion lyotropic liquid crystalline template as revealed by in situ XRD, SAXS, and XANES. J Phys Chem C 116:26649–26655. https://doi.org/10.1021/jp309622f

24. Chen X, Schröder J, Hauschild S, Rosenfeldt S, Dulle M, Förster S (2015) Simultaneous SAXS/WAXS/UV–vis study of the nucleation and growth of nanoparticles: a test of classical nucleation theory. Langmuir 31:11678–11691. https://doi.org/10.1021/acs.langmuir.5b02759
25. Tarasov A, Goertz V, Goodilin E, Nirschl H (2013) Hydrolytic stages of titania nanoparticles formation jointly studied by SAXS, DLS, and TEM. J Phys Chem C 117:12800–12805. https://doi.org/10.1021/jp312443u
26. Shard AG (2012) A straightforward method for interpreting XPS data from core–shell nanoparticles. J Phys Chem C 116:16806–16813. https://doi.org/10.1021/jp305267d
27. Sarma DD, Santra PK, Mukherjee S, Nag A (2013) X-ray photoelectron spectroscopy: a unique tool to determine the internal heterostructure of nanoparticles. Chem Mater 25:1222–1232. https://doi.org/10.1021/cm303567d
28. Barros WR, Steter JR, Lanza MR, Tavares AC (2016) Catalytic activity of $Fe_{3-x}Cu_xO4$ ($0 \leq x \leq 0.25$) nanoparticles for the degradation of Amaranth food dye by heterogeneous electro-Fenton process. Appl Catal B 180:434–441. https://doi.org/10.1016/j.apcatb.2015.06.048
29. Belsey NA, Shard AG, Minelli C (2015) Analysis of protein coatings on gold nanoparticles by XPS and liquid-based particle sizing techniques. Biointerphases 10:019012. https://doi.org/10.1116/1.4913566
30. Tunc I, Demirok UK, Suzer S, Correa-Duatre MA, Liz-Marzan LM (2005) Charging/discharging of Au (core)/silica (shell) nanoparticles as revealed by XPS. The J Phys Chem B 109:24182–24184. https://doi.org/10.1021/jp055614a
31. Prieto P, Nistor V, Nouneh K, Oyama M, Abd-Lefdil M, Díaz R (2012) XPS study of silver, nickel and bimetallic silver–nickel nanoparticles prepared by seed-mediated growth. Appl Surf Sci 258:8807–8813. https://doi.org/10.1016/j.apsusc.2012.05.095
32. Singh SC, Zeng HB, Guo C, Cai W (Eds.) (2012) Nanomaterials: processing and characterization with lasers. Wiley
33. Tobler DJ, Shaw S, Benning LG (2009) Quantification of initial steps of nucleation and growth of silica nanoparticles: An in-situ SAXS and DLS study. Geochim Cosmochim Acta 73:5377–5393. https://doi.org/10.1016/j.gca.2009.06.002
34. Lim J, Yeap SP, Che HX, Low SC (2013) Characterization of magnetic nanoparticle by dynamic light scattering. Nanoscale Res Lett 8: 381. https://link.springer.com/article/10.1186/1556-276X-8-381
35. Chicea D (2010) Nanoparticles and nanoparticle aggregates sizing by DLS and AFM. J Optoelectron Adv Mater 4:1310–1315
36. Lai YH, Koo S, Oh SH, Driskell EA, Driskell JD (2015) Rapid screening of antibody–antigen binding using dynamic light scattering (DLS) and gold nanoparticles. Anal 7:7249–7255. https://doi.org/10.1039/C5AY00674K
37. Murdock RC, Braydich-Stolle L, Schrand AM, Schlager JJ, Hussain SM (2008) Characterization of nanomaterial dispersion in solution prior to in vitro exposure using dynamic light scattering technique. Toxicol Sci 101:239–253. https://doi.org/10.1093/toxsci/kfm240
38. Dubiel M, Brunsch S, Seifert W, Hofmeister H, Tan GL (2001) Stress state of silver nanoparticles embedded in a silicate glass matrix investigated by HREM and EXAFS spectroscopy. Eur Phys J D 16: 229–232. https://link.springer.com/article/10.1007/s100530170098
39. Colthup N (2012) Introduction to infrared and Raman spectroscopy. Elsevier
40. Ferrari AC (2007) Raman spectroscopy of graphene and graphite: Disorder, electron–phonon coupling, doping and nonadiabatic effects. Solid State Commun 143:47–57. https://doi.org/10.1016/j.ssc.2007.03.052
41. Joshi M, Bhattacharyya A, Ali SW (2008) Characterization techniques for nanotechnology applications in textiles

42. Ahlawat A, Sathe VG, Reddy VR, Gupta A (2011) Mossbauer, Raman and X-ray diffraction studies of superparamagnetic NiFe2O4 nanoparticles prepared by sol–gel auto-combustion method. J Magn Magn Mater 323:2049–2054. https://doi.org/10.1016/j.jmmm.2011.03.017
43. Liu B, Zhou P, Liu X, Sun X, Li H, Lin M (2013) Detection of pesticides in fruits by surface-enhanced Raman spectroscopy coupled with gold nanostructures. Food Bioprocess Tech 6: 710–718. https://link.springer.com/article/10.1007/s11947-011-0774-5
44. Shukla N, Liu C, Jones PM, Weller D (2003) FTIR study of surfactant bonding to FePt nanoparticles. J Magn Magn Mater 266:178–184. https://doi.org/10.1016/S0304-8853(03)00469-4
45. Coates J (2006) Interpretation of infrared spectra, a practical approach. Encyclopedia of analytical chemistry: applications, theory and instrumentation
46. Shankar S, Rhim JW, Won K (2018) Preparation of poly (lactide)/lignin/silver nanoparticles composite films with UV light barrier and antibacterial properties. Int J Biol Macromol 107:1724–1731. https://doi.org/10.1016/j.ijbiomac.2017.10.038
47. Shankar S, Reddy JP, Rhim JW, Kim HY (2015) Preparation, characterization, and antimicrobial activity of chitin nanofibrils reinforced carrageenan nanocomposite films. Carbohydr Polym 117:468–475. https://doi.org/10.1016/j.carbpol.2014.10.010
48. Binnig G, Quate C F Gerber Ch 1986 Atomic force microscope. Phys Rev Lett 56: 930. https://iopscience.iop.org/article/10.1209/0295-5075/3/12/006/meta
49. Qiu H, Gao Y, Boott CE, Gould OE, Harniman RL, Miles MJ, Manners I (2016) Uniform patchy and hollow rectangular platelet micelles from crystallizable polymer blends. Science 352:697–701
50. De Moura MR, Mattoso LH, Zucolotto V (2012) Development of cellulose-based bactericidal nanocomposites containing silver nanoparticles and their use as active food packaging. J Food Eng 109:520–524. https://doi.org/10.1016/j.jfoodeng.2011.10.030
51. Dhar P, Bhasney SM, Kumar A, Katiyar V (2016) Acid functionalized cellulose nanocrystals and its effect on mechanical, thermal, crystallization and surfaces properties of poly (lactic acid) bionanocomposites films: A comprehensive study. Polymer 101:75–92. https://doi.org/10.1016/j.polymer.2016.08.028
52. Mazzaglia A, Scolaro LM, Mezzi A, Kaciulis S, Caro TD, Ingo GM, Padeletti G (2009) Supramolecular colloidal systems of gold nanoparticles/amphiphilic cyclodextrin: a FE-SEM and XPS investigation of nanostructures assembled onto solid surface. J Phys Chem C 113:12772–12777. https://doi.org/10.1021/jp903673x
53. de Britto D, de Moura MR, Aouada FA, Mattoso LH, Assis OB (2012) N, N, N-trimethyl chitosan nanoparticles as a vitamin carrier system. Food Hydrocoll 27:487–493. https://doi.org/10.1016/j.foodhyd.2011.09.002
54. Marbella LE, Millstone JE (2015) NMR techniques for noble metal nanoparticles. Chem Mater 27:2721–2739. https://doi.org/10.1021/cm504809c
55. Scheid D, Stock D, Winter T, Gutmann T, Dietz C, Gallei M (2016) The pivotal step of nanoparticle functionalization for the preparation of functional and magnetic hybrid opal films. J Phys Chem C 4:2187–2196. https://doi.org/10.1039/C5TC04388C
56. Hens Z, Martins JC (2013) A solution NMR toolbox for characterizing the surface chemistry of colloidal nanocrystals. Chem Mater 25:1211–1221. https://doi.org/10.1021/cm303361s
57. Sharma R, Taylor RE, Bouchard LS (2011) Intramolecular Ligand Dynamics in d 15-(PPh3)-Capped Gold Nanoparticles Investigated by 2H NMR. The J Phys Chem C 115:3297–3303. https://doi.org/10.1021/jp110686a
58. Smith AM, Marbella LE, Johnston KA, Hartmann MJ, Crawford SE, Kozycz LM, Millstone JE (2015) Quantitative analysis of thiolated ligand exchange on gold nanoparticles monitored by 1H NMR spectroscopy. Anal Chem 87:2771–2778. https://doi.org/10.1021/ac504081k
59. Andrade ÂL, Valente MA, Ferreira JM, Fabris JD (2012) Preparation of size-controlled nanoparticles of magnetite. J Magn Magn Mater 324:1753–1757. https://doi.org/10.1016/j.jmmm.2011.12.033

60. Galus S, Lenart A (2013) Development and characterization of composite edible films based on sodium alginate and pectin. J Food Eng 115:459–465. https://doi.org/10.1016/j.jfoodeng.2012.03.006
61. da Silva MA, Bierhalz ACK, Kieckbusch TG (2009) Alginate and pectin composite films crosslinked with Ca2+ ions: Effect of the plasticizer concentration. Carbohydr Polym 77:736–742. https://doi.org/10.1016/j.carbpol.2009.02.014
62. García MA, Pinotti A, Martino MN, Zaritzky NE (2009) Characterization of starch and composite edible films and coatings. In Edible films and coatings for food applications (pp. 169–209). Springer, New York, NY. https://link.springer.com/chapter/10.1007/978-0-387-92824-1_6
63. Siracusa V, Romani S, Gigli M, Mannozzi C, Cecchini JP, Tylewicz U, Lotti N (2018) Characterization of active edible films based on citral essential oil, alginate and pectin. Materials 11:1980. https://doi.org/10.3390/ma11101980
64. Acevedo-Fani A, Salvia-Trujillo L, Rojas-Graü MA, Martín-Belloso O (2015) Edible films from essential-oil-loaded nanoemulsions: Physicochemical characterization and antimicrobial properties. Food Hydrocoll 47:168–177. https://doi.org/10.1016/j.foodhyd.2015.01.032
65. Rojas-Graü MA, Avena-Bustillos RJ, Olsen C, Friedman M, Henika PR, Martín-Belloso O, McHugh TH (2007) Effects of plant essential oils and oil compounds on mechanical, barrier and antimicrobial properties of alginate–apple puree edible films. Journal J Food Eng 81:634–641. https://doi.org/10.1016/j.jfoodeng.2007.01.007
66. McHugh TH, Krochta JM (1994) Sorbitol-vs glycerol-plasticized whey protein edible films: integrated oxygen permeability and tensile property evaluation. J Agric Food Chem 42: 841–845. https://pubs.acs.org/doi/pdf/10.1021/jf00040a001
67. Mondal K, Ghosh T, Bhagabati P, Katiyar V (2019) Sustainable nanostructured materials in food packaging. In: Dynamics of advanced sustainable nanomaterials and their related nanocomposites at the bio-nano interface, pp 171–213, Elsevier
68. Yoo S, Krochta JM (2011) Whey protein–polysaccharide blended edible film formation and barrier, tensile, thermal and transparency properties. J Sci Food Agric 91:2628–2636. https://doi.org/10.1002/jsfa.4502
69. Saberi B, Thakur R, Vuong QV, Chockchaisawasdee S, Golding JB, Scarlett CJ, Stathopoulos CE (2016) Optimization of physical and optical properties of biodegradable edible films based on pea starch and guar gum. Ind Crops Prod 86:342–352. https://doi.org/10.1016/j.indcrop.2016.04.015
70. Sohail SS, Wang B, Biswas MA, Oh JH (2006) Physical, morphological, and barrier properties of edible casein films with wax applications. J Food Sci 71:C255–C259. https://doi.org/10.1111/j.1750-3841.2006.00006.x
71. Sun Q, Sun C, Xiong L (2013) Mechanical, barrier and morphological properties of pea starch and peanut protein isolate blend films. Carbohydr Res 98:630–637. https://doi.org/10.1016/j.carbpol.2013.06.040
72. Ghasemlou M, Khodaiyan F, Oromiehie A, Yarmand MS (2011) Development and characterisation of a new biodegradable edible film made from kefiran, an exopolysaccharide obtained from kefir grains. Food Chem 127:1496–1502. https://doi.org/10.1016/j.foodchem.2011.02.003
73. Martins JT, Bourbon AI, Pinheiro AC, Souza BW, Cerqueira MA, Vicente AA (2013) Biocomposite films based on κ-carrageenan/locust bean gum blends and clays: physical and antimicrobial properties. Food Bioprocess Tech 6: 2081–2092. https://link.springer.com/article/10.1007/s11947-012-0851-4
74. Coupland JN, Shaw NB, Monahan FJ, O'Riordan ED, O'Sullivan M (2000) Modeling the effect of glycerol on the moisture sorption behavior of whey protein edible films. J Food Eng 43:25–30. https://doi.org/10.1016/S0260-8774(99)00129-6
75. Peressini D, Bravin B, Lapasin R, Rizzotti C, Sensidoni A (2003) Starch–methylcellulose based edible films: rheological properties of film-forming dispersions. J Food Eng 59:25–32. https://doi.org/10.1016/S0260-8774(02)00426-0

76. AOAC (2010) Official Methods of Analysis. 18th Edition, Revision 3, Association of Official Analytical Chemists, Washington, DC
77. Zhang L, Chen F, Lai S, Wang H, Yang H (2018) Impact of soybean protein isolate-chitosan edible coating on the softening of apricot fruit during storage. LWT 96:604–611. https://doi.org/10.1016/j.lwt.2018.06.011
78. Mannozzi C, Tylewicz U, Chinnici F, Siroli L, Rocculi P, Dalla Rosa M, Romani S (2018) Effects of chitosan based coatings enriched with procyanidin by-product on quality of fresh blueberries during storage. Food Chem 251:18–24. https://doi.org/10.1016/j.foodchem.2018.01.015
79. Mahajan PV, Goswami TK (2001) PH—Postharvest technology: enzyme kinetics based modelling of respiration rate for apple. J Agric Eng Res 79:399–406. https://doi.org/10.1006/jaer.2001.0718
80. Ravindra MR, Goswami TK (2008) Modelling the respiration rate of green mature mango under aerobic conditions. Biosyst Eng 99:239–248. https://doi.org/10.1016/j.biosystemseng.2007.10.005
81. Fonseca SC, Oliveira FA, Brecht JK (2002) Modelling respiration rate of fresh fruits and vegetables for modified atmosphere packages: a review. J Food Eng 52:99–119. https://doi.org/10.1016/S0260-8774(01)00106-6
82. Bhande SD, Ravindra MR, Goswami TK (2008) Respiration rate of banana fruit under aerobic conditions at different storage temperatures. J Food Eng 87:116–123. https://doi.org/10.1016/j.jfoodeng.2007.11.019
83. Heydari AMIR, Shayesteh K, Eghbalifam N, Bordbar HOSSEIN, Falahatpisheh S (2010) Studies on the respiration rate of banana fruit based on enzyme kinetics. Int J Agric Biol 12:145–149
84. Pinheiro J, Alegria C, Abreu M, Gonçalves EM, Silva CL (2013) Kinetics of changes in the physical quality parameters of fresh tomato fruits (Solanum lycopersicum, cv. 'Zinac') during storage. J Food Eng 114:338–345. https://doi.org/10.1016/j.jfoodeng.2012.08.024
85. Mangaraj S, Goswami TK (2011) Modeling of respiration rate of litchi fruit under aerobic conditions. Food Bioprocess Technol 4:272. https://doi.org/10.1007/s11947-008-0145-z
86. Ghosh T, Dash KK (2020) Modeling on respiration kinetics and modified atmospheric packaging of fig fruit. J Food Meas Charact 1–13:1092–1104. https://doi.org/10.1007/s11694-019-00359-2
87. Ghosh T, Dash KK (2018) Respiration rate model and modified atmosphere packaging of bhimkol banana. Eng Agric, Environ Food 11:186–195. https://doi.org/10.1016/j.eaef.2018.04.004
88. Dadzie BK, Banks NH, Cleland DJ, Hewett EW (1996) Changes in respiration and ethylene production of apples in response to internal and external oxygen partial pressures. Postharvest Biol Tec 9:297–309. https://doi.org/10.1016/S0925-5214(96)00030-0
89. Benítez S, Chiumenti M, Sepulcre F, Achaerandio I, Pujolá M (2012) Modeling the effect of storage temperature on the respiration rate and texture of fresh cut pineapple. J Food Eng 113:527–533. https://doi.org/10.1016/j.jfoodeng.2012.07.022
90. Wang ZW, Duan HW, Hu CY (2009) Modelling the respiration rate of guava (Psidium guajava L.) fruit using enzyme kinetics, chemical kinetics and artificial neural network. Eur Food Res Technol 229:495–503. https://doi.org/10.1007/s00217-009-1079-z
91. Cameron AC, Beaudry RM, Banks NH, Yelanich MV (1994) Modified-atmosphere packaging of blueberry fruit: modeling respiration and package oxygen partial pressures as a function of temperature. J Am Soc Hortic Sci 119:534–539. https://doi.org/10.21273/JASHS.119.3.534
92. Sherman P (1975) Textural properties and food acceptability. Proceedings of the Royal Society of London. Series B. Biol Sci 191:131–144. https://doi.org/10.1098/rspb.1975.0117
93. Bourne M (2009) Texture in solid and semisolid foods. Food Eng-Vol I II:224
94. Chen L, Opara UL (2013) Approaches to analysis and modeling texture in fresh and processed foods–A review. J Food Eng 119:497–507. https://doi.org/10.1016/j.jfoodeng.2013.06.028

95. Jeltema M, Beckley J, Vahalik J (2015) Model for understanding consumer textural food choice. Food Sci Nutr 3:202–212. https://doi.org/10.1002/fsn3.205
96. Singh V, Guizani N, Al-Alawi A, Claereboudt M, Rahman MS (2013) Instrumental texture profile analysis (TPA) of date fruits as a function of its physico-chemical properties. Ind Crops Prod 50:866–873. https://doi.org/10.1016/j.indcrop.2013.08.039
97. Kohyama K (2020) Food Texture–Sensory Evaluation and Instrumental Measurement. Textural Charact World Foods, 1–13. https://doi.org/10.1002/9781119430902.ch1
98. Souza VGL, Fernando AL (2016) Nanoparticles in food packaging: Biodegradability and potential migration to food—A review. Food Packag Shelf Life 8:63–70. https://doi.org/10.1016/j.fpsl.2016.04.001
99. Silva AS, Cruz JM, Garcı RS, Franz R, Losada PP (2007) Kinetic migration studies from packaging films into meat products. Meat Sci 77:238–245. https://doi.org/10.1016/j.meatsci.2007.03.009
100. Chung D, Papadakis SE, Yam KL (2002) Simple models for assessing migration from food-packaging films. Food Addit Contam 19:611–617. https://doi.org/10.1080/02652030210126389
101. Ghosh T, Bhasney SM, Katiyar V (2020) Blown films fabrication of poly lactic acid based biocomposites: Thermomechanical and migration studies. Mater Today Commun 22:100737. https://doi.org/10.1016/j.mtcomm.2019.100737
102. Commission European (2011) Commission Regulation (EC) No. 10/2011 on plastic materials and articles intended to come into contact with food. Off J Eur Union, L 12:1–89
103. Begley TH, White K, Honigfort P, Twaroski ML, Neches R, Walker RA (2005) Perfluorochemicals: potential sources of and migration from food packaging. Food Addit Contam 22:1023–1031. https://doi.org/10.1080/02652030500183474
104. Nerín C, Asensio E (2007) Migration of organic compounds from a multilayer plastic–paper material intended for food packaging. Anal Bioanal Chem 389:589–596. https://doi.org/10.1007/s00216-007-1462-1
105. Nerin C, Acosta D, Rubio C (2002) Potential migration release of volatile compounds from plastic containers destined for food use in microwave ovens. Food Addit Contam 19:594–601. https://doi.org/10.1080/02652030210123887
106. Papilloud S, Baudraz D (2002) Analysis of food packaging UV inks for chemicals with potential to migrate into food simulants. Food Addit Contam 19:168–175. https://doi.org/10.1080/02652030110084800
107. Aznar M, Vera P, Canellas E, Nerín C, Mercea P, Störmer A (2011) Composition of the adhesives used in food packaging multilayer materials and migration studies from packaging to food. J Mater Chem 21:4358–4370. https://doi.org/10.1039/C0JM04136J
108. Nerín C, Contín E, Asensio E (2007) Kinetic migration studies using Porapak as solid-food simulant to assess the safety of paper and board as food-packaging materials. Anal Bioanal Chem 387:2283–2288. https://doi.org/10.1007/s00216-006-1080-3
109. Echegoyen Y, Rodríguez S, Nerín C (2016) Nanoclay migration from food packaging materials. Food Addit Contam Part A 33:530–539. https://doi.org/10.1080/19440049.2015.1136844
110. Addo Ntim S, Thomas TA, Begley TH, Noonan GO (2015) Characterisation and potential migration of silver nanoparticles from commercially available polymeric food contact materials. Food Addit Contam Part A 32:1003–1011. https://doi.org/10.1080/19440049.2015.1029994
111. Guerreiro TM, de Oliveira DN, Melo CFOR, de Oliveira Lima E, Catharino RR (2018) Migration from plastic packaging into meat. Food Res Int 109:320–324. https://doi.org/10.1016/j.foodres.2018.04.026